Near- and Mid-IR Integrated Photonics for Sensing, Interconnects and Computing

Ray T. Chen
Microelectronics Research Center
The University of Texas, Austin
Austin, TX 78758
&
Omega Optics Inc.

http://www.mrc.utexas.edu/people/faculty/ray-chen
www.omegaoptics.com

5/7/2024

This Research Has Been Supported by

NSF

AFOSR/AFRL

ONR

US Army

DARPA

NASA

NIST

DOE

EPA

NIH

Omega Optics

State of Texas

Table of Contents:

Integrated Photonics application range 2024 & Beyond

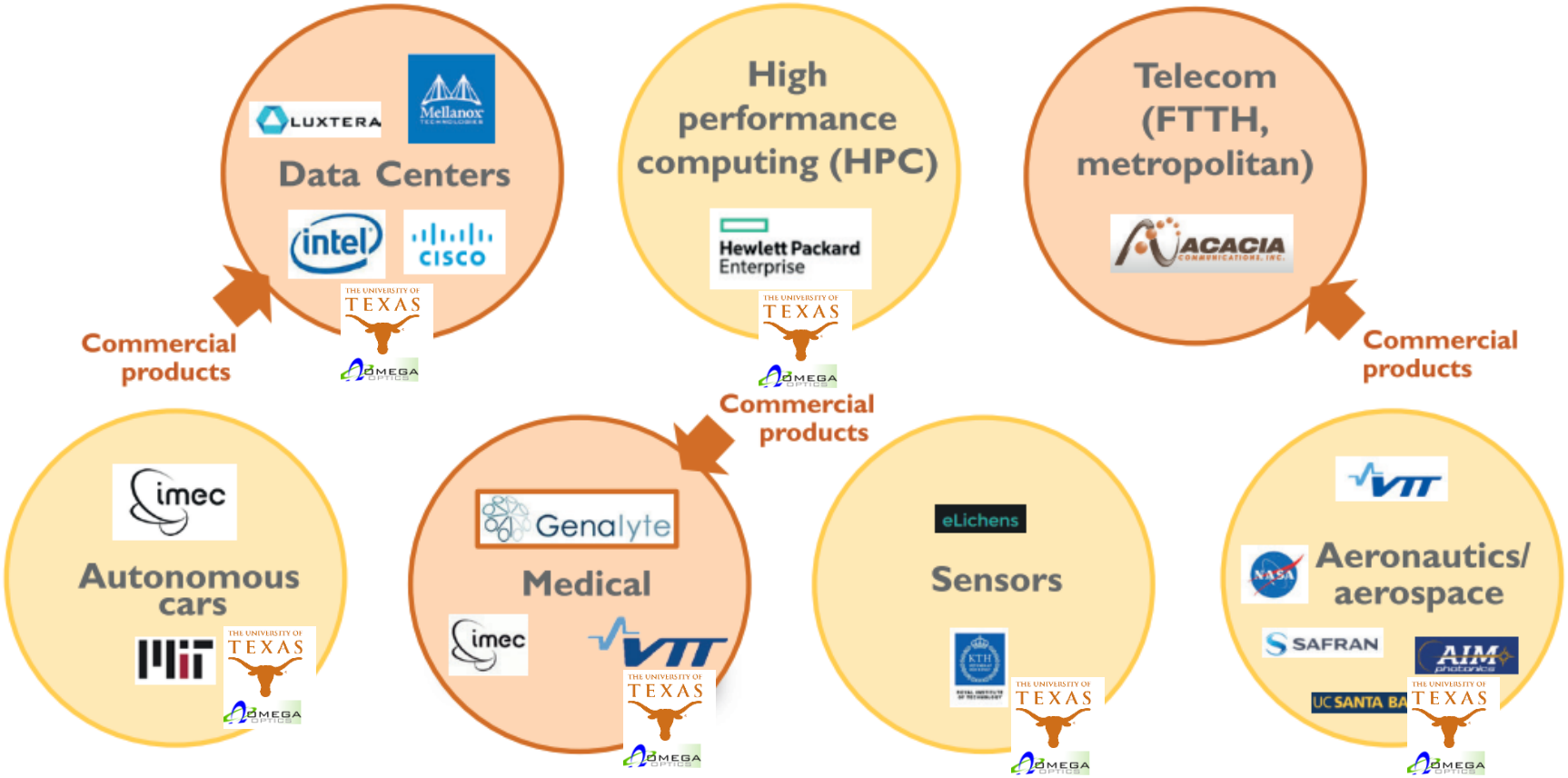

(Yole Développement, January 2018)

Table of Contents:

Photonic Crystals and Defects

Periodic atomic structure (Natural)

Electronic Bandgap

Semiconductors

Introduction of defects

Trapped Carriers

Schrődinger Equation

$$\left(\frac{p^2}{2m}+V(\vec{r})\right)\Psi_E(\vec{r})=E\Psi_E(\vec{r})$$

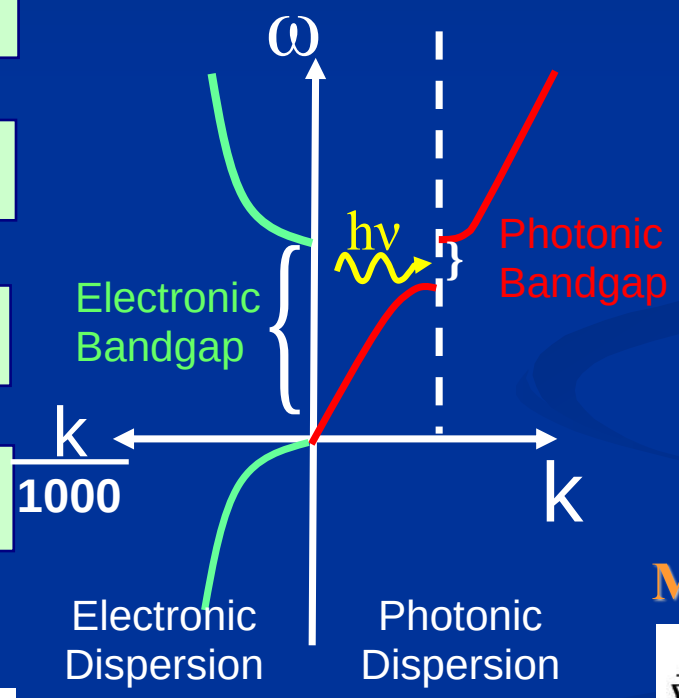

Eigenvalue Problem

Periodic variation of refractive index (Artificial)

Photonic Bandgap

Photonic Crystals

Introduction of defects

PC resonant cavities and waveguides

Maxwell's Equations

$$\vec{\nabla}\times\left[\frac{1}{\varepsilon(\vec{r})}\vec{\nabla}\times\vec{H}(\vec{r})\right]=\left(\frac{\omega}{c}\right)^2\vec{H}(\vec{r})$$

$$\vec{\nabla}\cdot\vec{H}(\vec{r})=0$$

Silicon Nanophotonic Biosensor Chip for Lung Cancer Detection

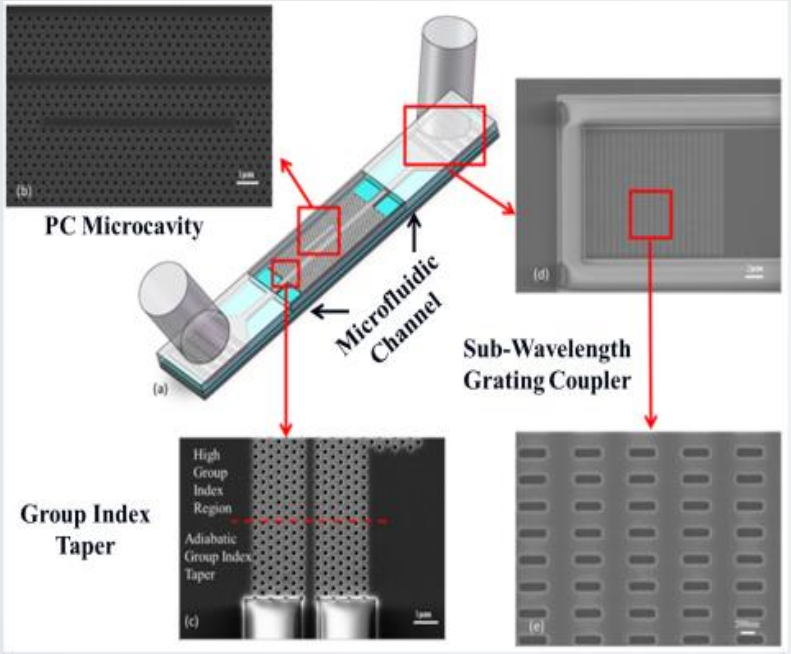

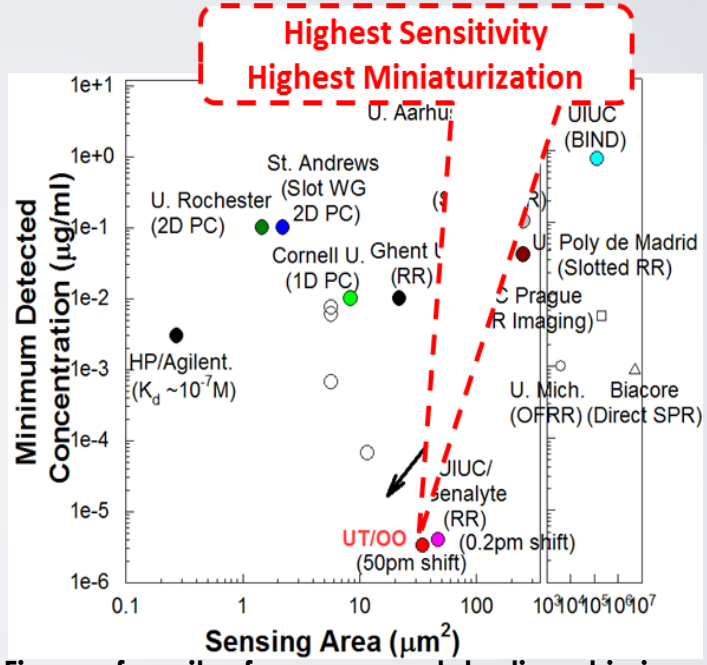

Figure of merits of our cancer detection chip in reference to all existing results [1-12]

[1] J. Waswa, J. Irudayaraj, C. Deb Roy, "Direct detection of E-Coli O157: H7 in selected food systems by a surface plasmon resonance biosensor", LWT-Food Science and Technology **40** (2), 187 (2007).
[2] M.G. Scullion, et al., "Slotted photonic crystal cavities with integrated microfluidics for biosensing applications", Biosens. Bioelectron. **27**, 101-105 (2011).
[3] S. Mandal, D. Erickson, "Nanoscale optofluidic sensor arrays", Opt. Exp.**16**(3), 1623 (2008).
[4] S. Pal, et al., "Silicon photonic crystal nanocavity-coupled waveguides for error-corrected optical biosensing", Biosens. Bioelectron. **26**, 4024 (2011).
[5] C.F. Carlborg, et. al, "A packaged optical slot-waveguide ring resonator sensor array for multiplex label-free assays in labs-on-chips", Lab on a Chip **10**, 281 (2010).
[6] K. De Vos, et al., "Silicon-on-insulator microring resonator for sensitive and label-free biosensing", Opt. Exp. **15** (12), 7610 (2007).
[7] C.A. Barrios, "Optical slot-waveguide based biochemical sensors", Sensors **9**, 4751 (2009).
[8] S. Zlatanovic, et al., "Photonic crystal microcavity sensor for ultracompact monitoring of reaction kinetics and protein concentration", Sens. and Actuators B **141**, 13-19 (2009).
[9] H. Li, X. Fan, "Characterization of sensing capability of optofluidic ring resonator biosensors", Appl. Phys. Lett. **97**, 011105 (2010).
[10] B.T. Cunningham, et al, "Label-free assays on the BIND system", J. Biomol. Screen. **9**, 481 (2004).
[11] M. Iqbal, et al., "Label-Free Biosensor Arrays based on silicon ring resonators and high-speed optical scanning instrumentation", IEEE J. Sel. Top. Quant. Electron. **16**(3), 654 (2010).
[12] Y. Zou, S. Chakravarty, W-C. Lai, R.T. Chen, "High yield silicon photonic crystal microcavity biosensors with 100fM detection limit", Proc. of the SPIE 8570, 857008 (2013) and S. Chakravarty, Y. Zou, W-C. Lai, R.T. Chen, "Slow light engineering for high Q high sensitivity photonic crystal microcavity biosenors in silicon", Biosensors and Bioelectronics 38(1), 170 (2012).

Biochip Preparation and Detection Procedure

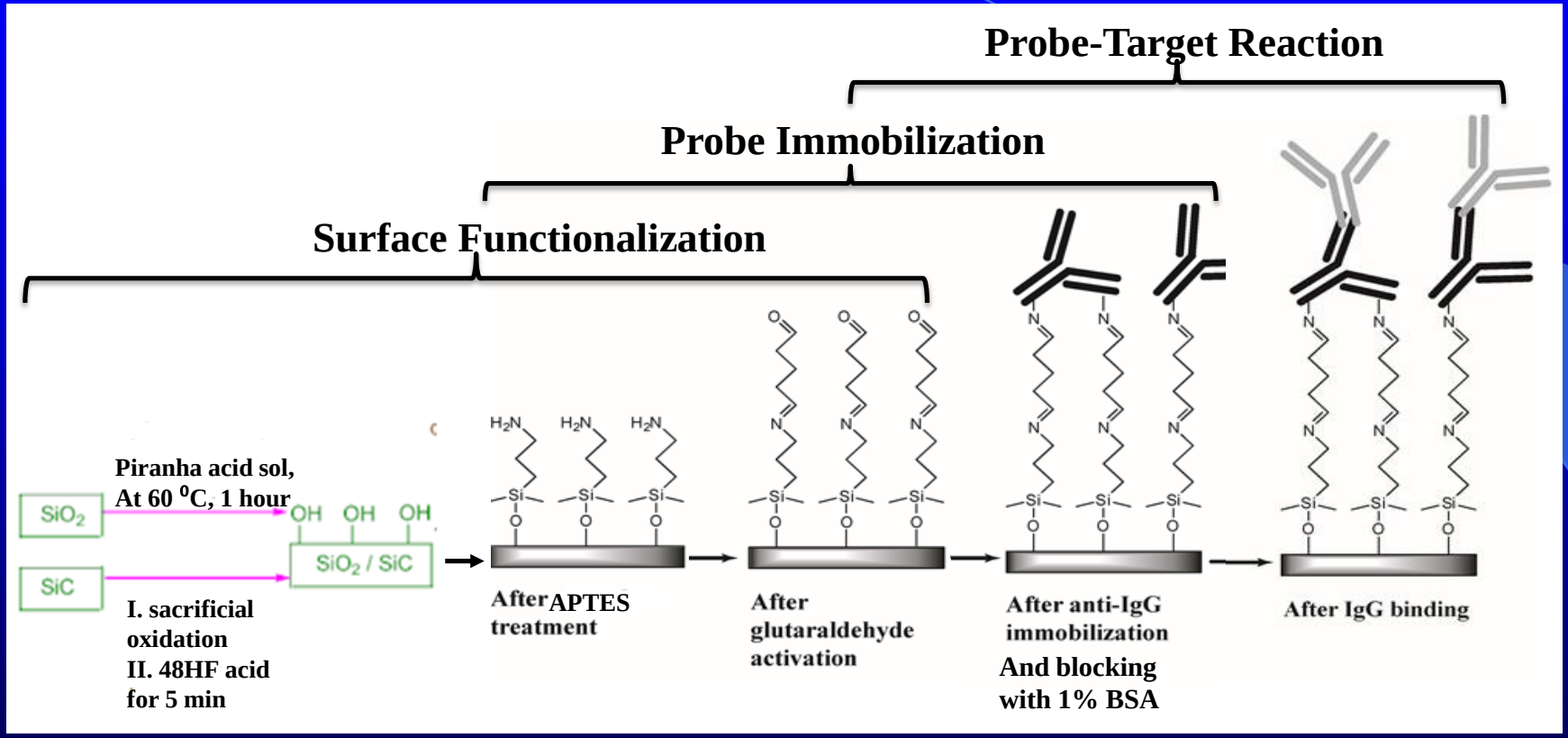

Integrated Photonics for Biosensing

(Lab-on-chip)

Subwavelength grating microring resonator (SWGMR)

Cancer Treatment

Cancer Screening

COVID-19 Detection

Heavy Metal Detection

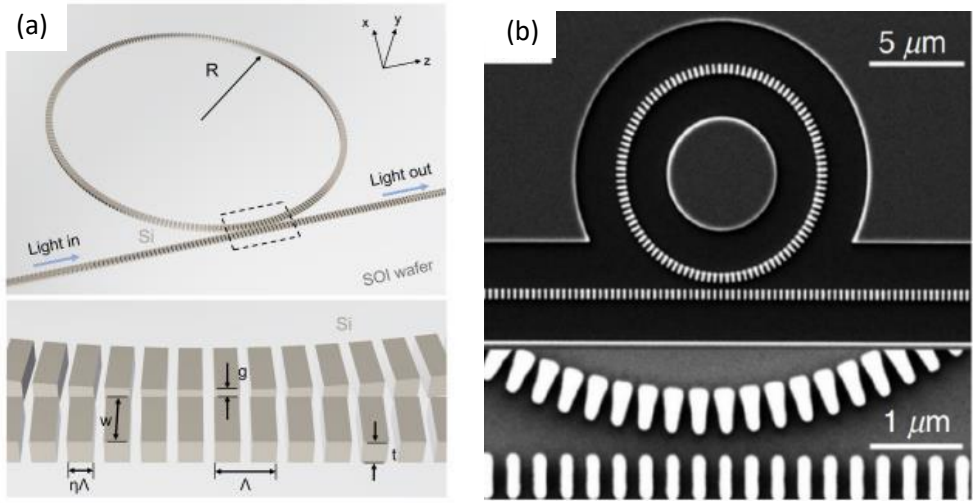

Figure: Schematic of SWGMR biosensor. (a). Device schematic (b). Real fabrication.

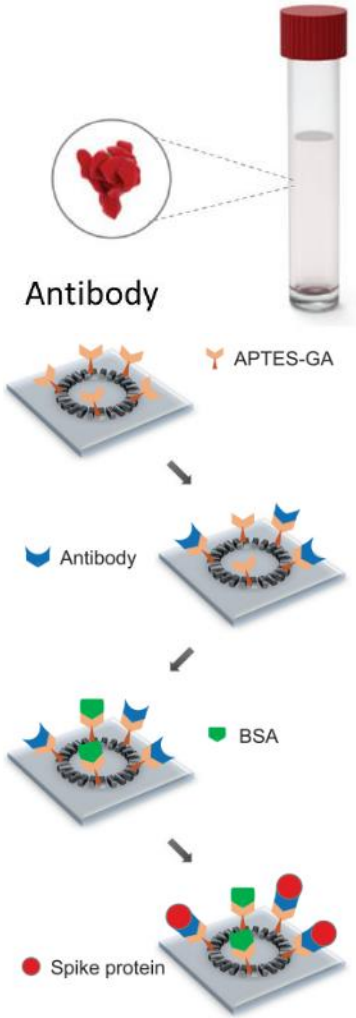

Figure: surface functionalization of SWGMR.

Figure: Biosensor test bench. A platform for the detection of biomarker

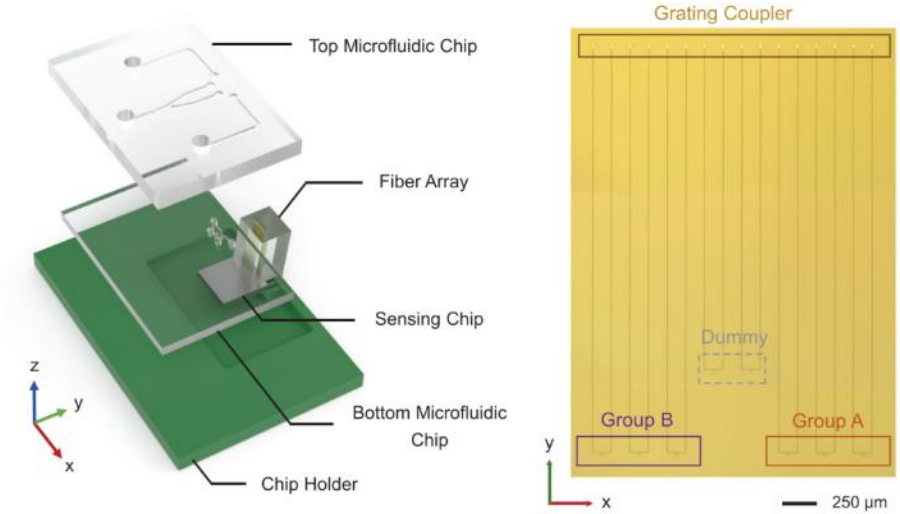

Figure: Biosensor cartridge / Silicon photonics biosensing chip

LabVIEW-based Program for Peak Detection

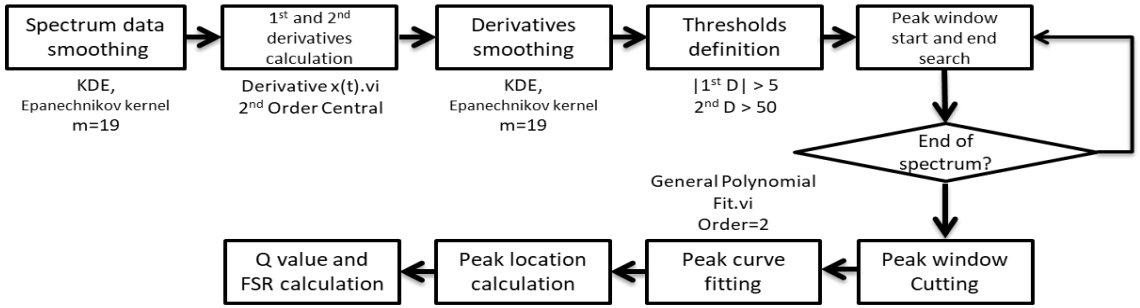

Figure: Flowchart of the peak minimum location determination algorithm.

$$T_{ap}(\phi_{rt}) = \frac{T_{ap,min} + F\sin^2(\frac{\phi_{rt}}{2})}{1 + F\sin^2(\frac{\phi_{rt}}{2})}$$

T_{ap}: power transfer, ϕ_{rt}: roundtrip phase detune

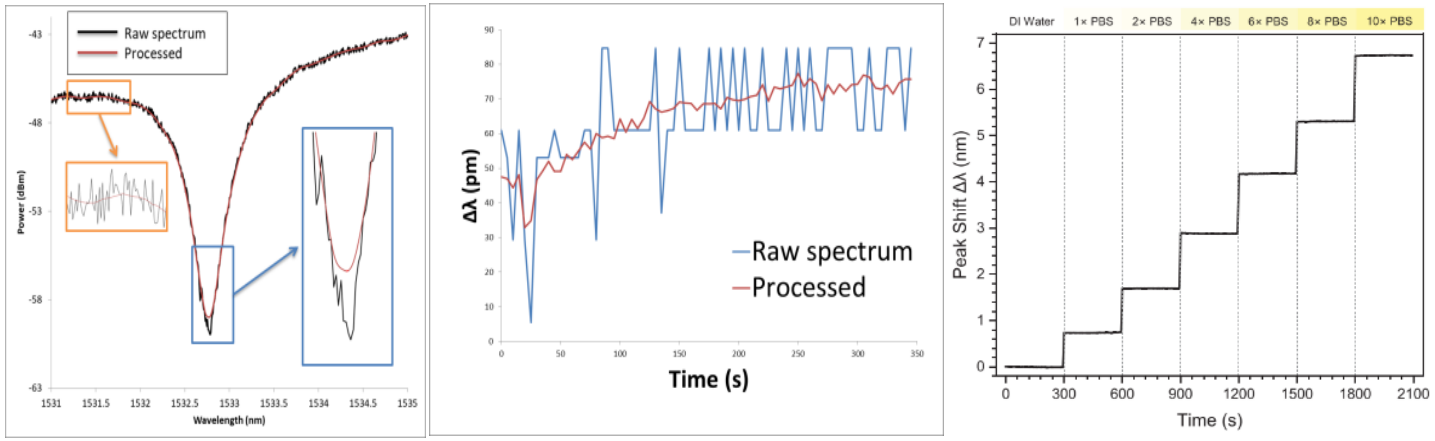

Figure: (a) The high noise real bio sensing spectrum. (b) Real-time Δλ analysis with algorithm implemented. (c) Real-time peak shift tracking

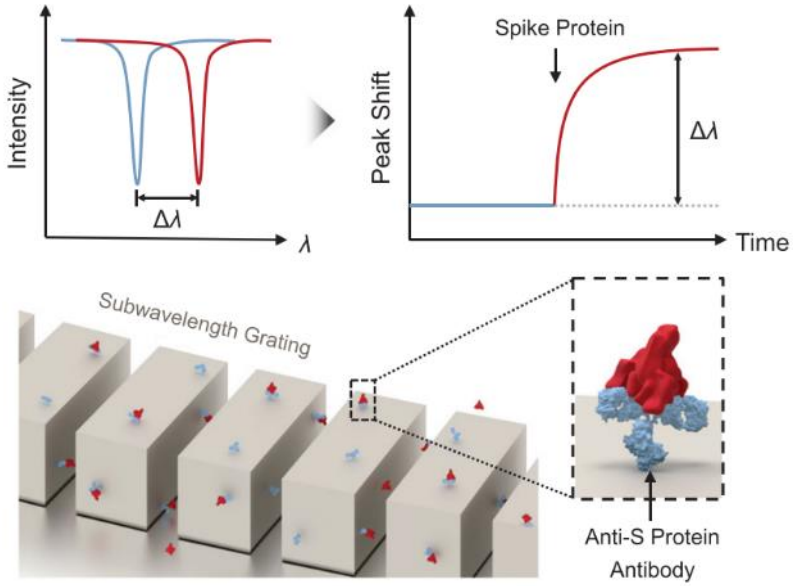

Figure: Spike antibodies (blue) are conjugated on SUMIRRs as specific probes. Tracking the redshift of resonant peaks

Strong Partners

- **Medical cancer clinics**
  - MD Anderson
  - Medical University of South Carolina
  - Louisiana State University Health Science Center
- **Pancreatic Cancer in US today: 65,000 cases**
  - Survival rate at early detection: 44%
  - Overall survival rate today: 15%
- **With Our Bio-Photonic chip's early detection**
  - Converts all cases to early detection cases
  - Overall survival rate improves by 29% (from 15% to 44%)
  - Increased survivors: 65,000 * 29% = 18,500

THE UNIVERSITY OF TEXAS MD Anderson Cancer Center®

MUSC Medical University of South Carolina

LSU Health NEW ORLEANS

50 lives saved every day

on just pancreatic cancer in the US alone

20 US Patents Granted

1 Two-dimensional photonic crystal MicroArray measurement method and apparatus for highly-sensitive label-free multiple analyte sensing, biosensing, and diagnostic assay
US Patent number: 11097246, 2021
2 Two-dimensional photonic crystal microarray measurement method and apparatus for highly-sensitive label-free multiple analyte sensing, biosensing, and diagnostic assay
US Patent number: 10610846, 2020
3 Subwavelength Photonic Crystal Waveguide in Optical Systems
US Patent 10,215,918, 2019
4 Method for label-free multiple analyte sensing, biosensing and diagnostic assay
US Patent number: 9579621, 2013
5 Subwavelength photonic crystal waveguide with trapezoidal shaped dielectric pillars in optical systems
US Patent number: 9563016, 2017
6 Subwavelength grating coupler
US Patent number: 9122820, 2015
7 Method for chip-integrated label-free detection and absorption spectroscopy with high throughput, sensitivity, and specificity
US Patent number: 9063135, 2015
8 Broadband, Group Index Independent, and Ultra-Low Loss Coupling into Slow Light Slotted Photonic Crystal Waveguides
US Patent 9,170,374, 2015
9 Packaged Chip For Multiplexing Photonic Crystal Microcavity Coupled Waveguide And Photonic Crystal Slot Waveguide Devices For Chip-Integrated Label-Free Detection And Absorption Spectroscopy With High Throughput, Sensitivity, Specificity, And Wide Dynamic Range
US Patent 9,164,026, 2015
10 Packaged chip for multiplexing photonic crystal waveguide and photonic crystal slot waveguide devices for chip-integrated label-free detection and absorption spectroscopy with high throughput, sensitivity, and specificity
US Patent number: 8636955, 2014
11 Photonic crystal microarray layouts for enhanced sensitivity and specificity of label-free multiple analyte sensing, biosensing and diagnostic assay
US Patent number: 8623284, 2014
12 Method for label-free multiple analyte sensing, biosensing and diagnostic assay
US Patent number: 8580200, 2013
13 Photonic crystal band-shifting device for dynamic control of light transmission
US Patent number: 8571373, 2013
14 Photonic crystal microarray device for label-free multiple analyte sensing, biosensing and diagnostic assay chips
US Patent 8,293,177, 2012
15 Multimode interference coupler for use with slot photonic crystal waveguides
US Patent number: 8189968, 2012
16 Photonic crystal band-shifting device for dynamic control of light transmission
US Patent App. 12/455,791, 2010
17 Method for the chip-integrated spectroscopic identification of solids, liquids, and gases
US Patent number: 9157850, 2015
18 Method for the chip-integrated spectroscopic identification of solids, liquids, and gases
US Patent 8,585,974, 2013
19 Integrated photonic crystal structures and their applications
US Patent 9,157,856, 2015
20 Slot waveguide with structural modulation
US Patent number: 10490906, 2019

Biomarkers so far has been detected

Breast cancer biomarkers
Lung Cancer Biomarkers
Pancreatic Cancer Biomarkers
Three Antibiotic drugs
Heavy metal attached biomarkers
COVID-19 Spike Proteins
Flu virus
Depression biomarker (under evaluation)

Table of Contents:

Absorption Spectroscopy

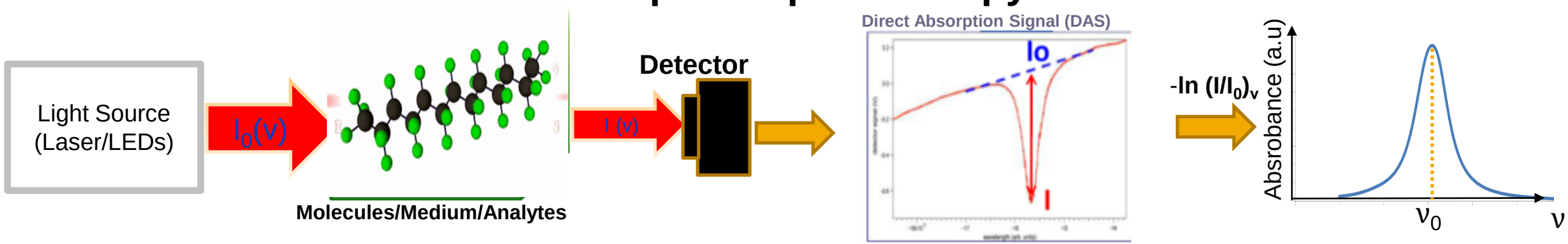

Conventional Infrared (IR) Spectroscopy

✔ Benefits

- Highly sensitive and selective measurement
- Real-time detection

✗ Issues

- Bulky
- Alignment Sensitive
- Expensive
- Desktop usage only

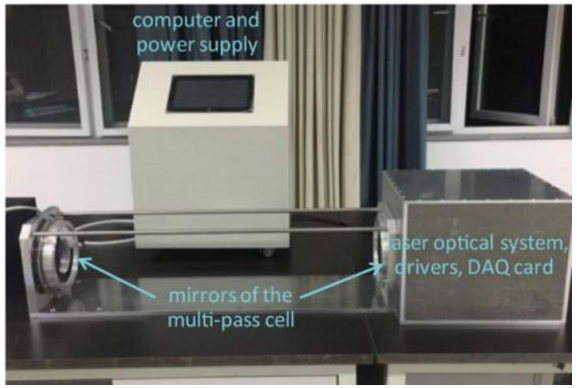

Chen Xiang et. al. C *Physics B* 27, no. 4 (2018)

Beer-Lambert's law

$$I(\nu) = I_0 \cdot e^{-\Upsilon \alpha(\nu) L}$$

$$S = Absorbance = ln\left(\frac{I(\nu)}{I_0}\right) = -\Upsilon \alpha(\nu) L = -\Upsilon n \overline{\sigma(\nu)} L$$

$$\Upsilon = f \times \frac{\frac{c}{n}}{v_g}$$

$\alpha(\nu)$: the absorption coefficient, Υ : the medium-specific absorption factor
f : the filling factor; v_g : group velocity; n_g : group index,

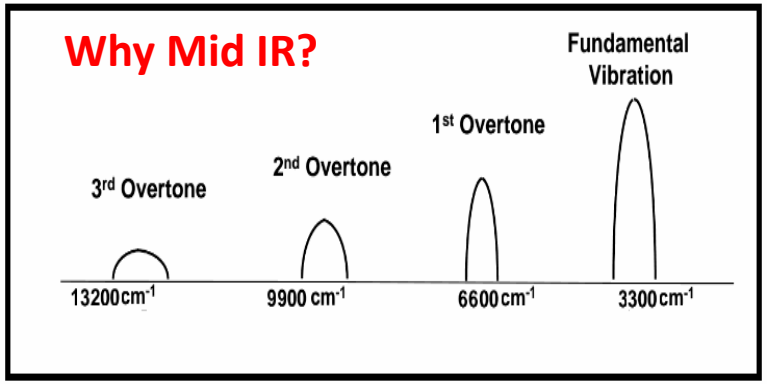

Miniaturized Lab-on-chip Absorption Spectroscopy

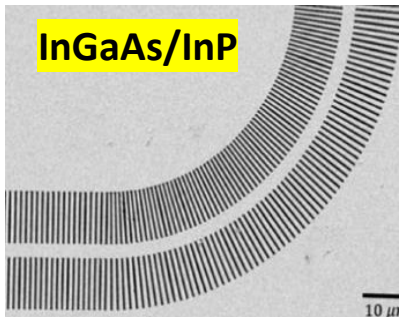

Yoo, Kyoung Min, et al. *ACS sensors* 5.3 (2020): 861-869.

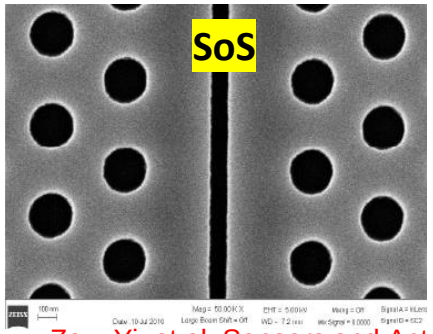

Zou, Yi, et al. Sensors and Actuators B: Chemical 221 (2015): 1094-1103.

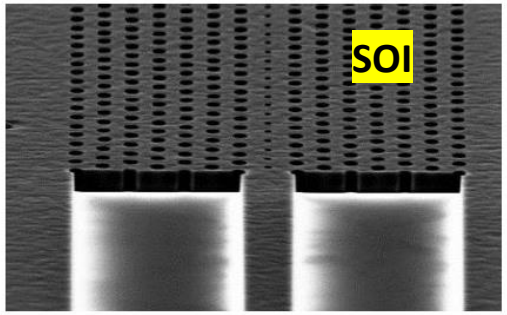

Rostamian, Ali, et al. Nanophotonics 10.6 (2021): 1675-1682.

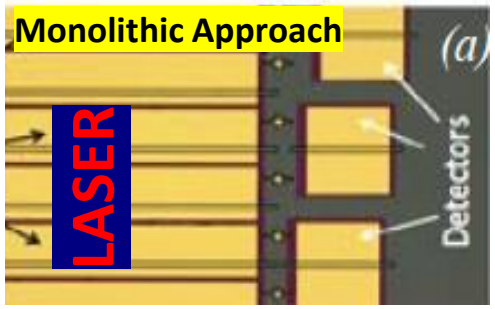

Zou, Yi, et al. 2015 CLEO IEEE, 2015.

Detected Analytes (on-chip)

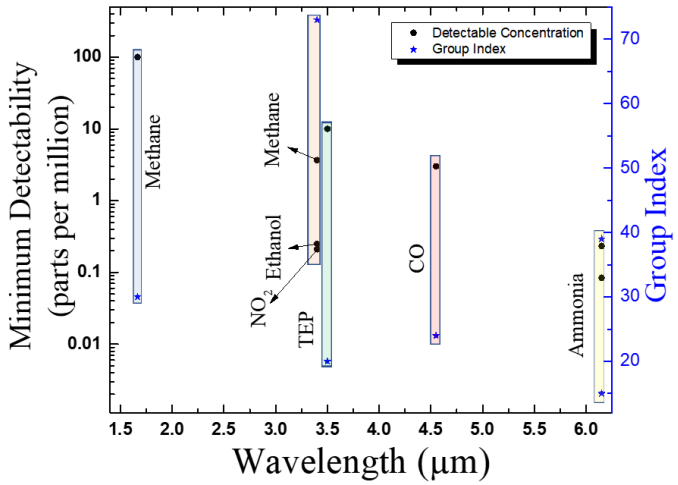

Dispersion relation in a periodic structure

- phase velocity : $v = \frac{\omega}{k}$
- group velocity : $v_g = \frac{d\omega}{dk}$
- the group index : $n_g = \frac{c}{v_g} = c/\left(\frac{d\omega}{dk}\right)$
  - a slow-down factor from the velocity, *c*.

Effective pathlength (L_{eff}) → physical chip length (L) x group index (n_g)

Overall light-analyte interaction → L_{eff}×optical confinement in the air

$n_g \uparrow$ $V_g \downarrow$ $\gamma \uparrow \rightarrow \Delta I \rightarrow$ **Better Sensitivity**

Parameters	MOS Resistive sensor	Electrochemical sensor	On-Chip Spectroscopy
Sensitivity	Moderate (in sub ppm)	Moderate (in sub ppm)	High (in ppb level)
Selectivity	Poor	Moderate	High
Power consumption	Low (≈ 60-80 mW)	Low (≈20-50 mW)	Low (in tens of mW)
life-time	≈ 3-8 Years	**≈5-10 Years**	> 25 Years
Sensor Size	≈1 cm3	≈ 3.5 cm3	≈ 2 cm3 (multiplexed)
Weight	Light	Light	Light
Cost	Low (typically <$50)	High	Low (expected <$30)
warm up required	Yes (typically <45 Sec)	Yes (<typically 10 Sec)	No
Portability	Yes	Yes	Yes

On-Chip Fourier Transform Spectroscopy

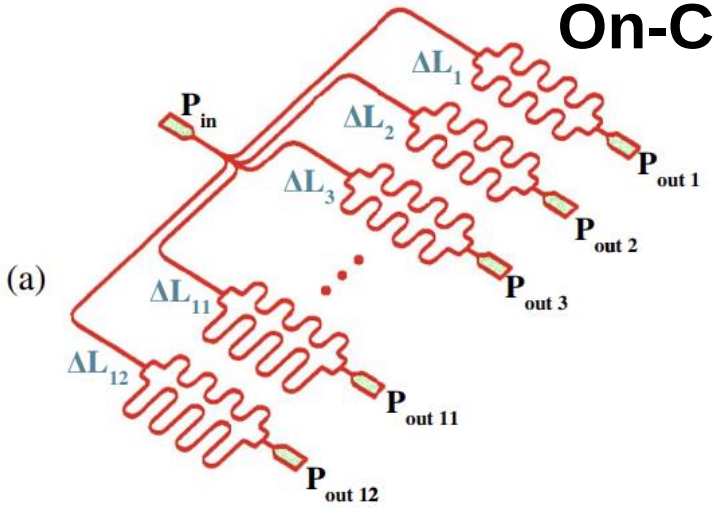

Heidari, Elham, et al. Optics Letters 44.11 (2019): 2883-2886.

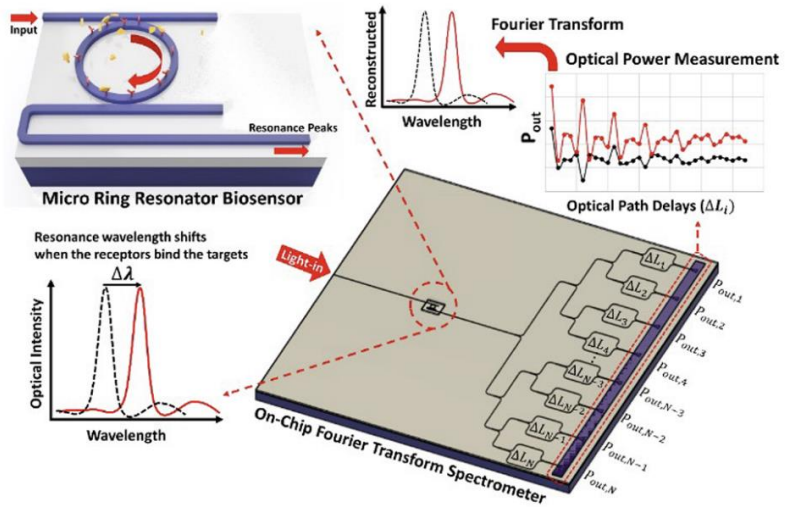

Yoo, Kyoung Min, et al. Optics Letters 48.20 (2023): 5371-5374.

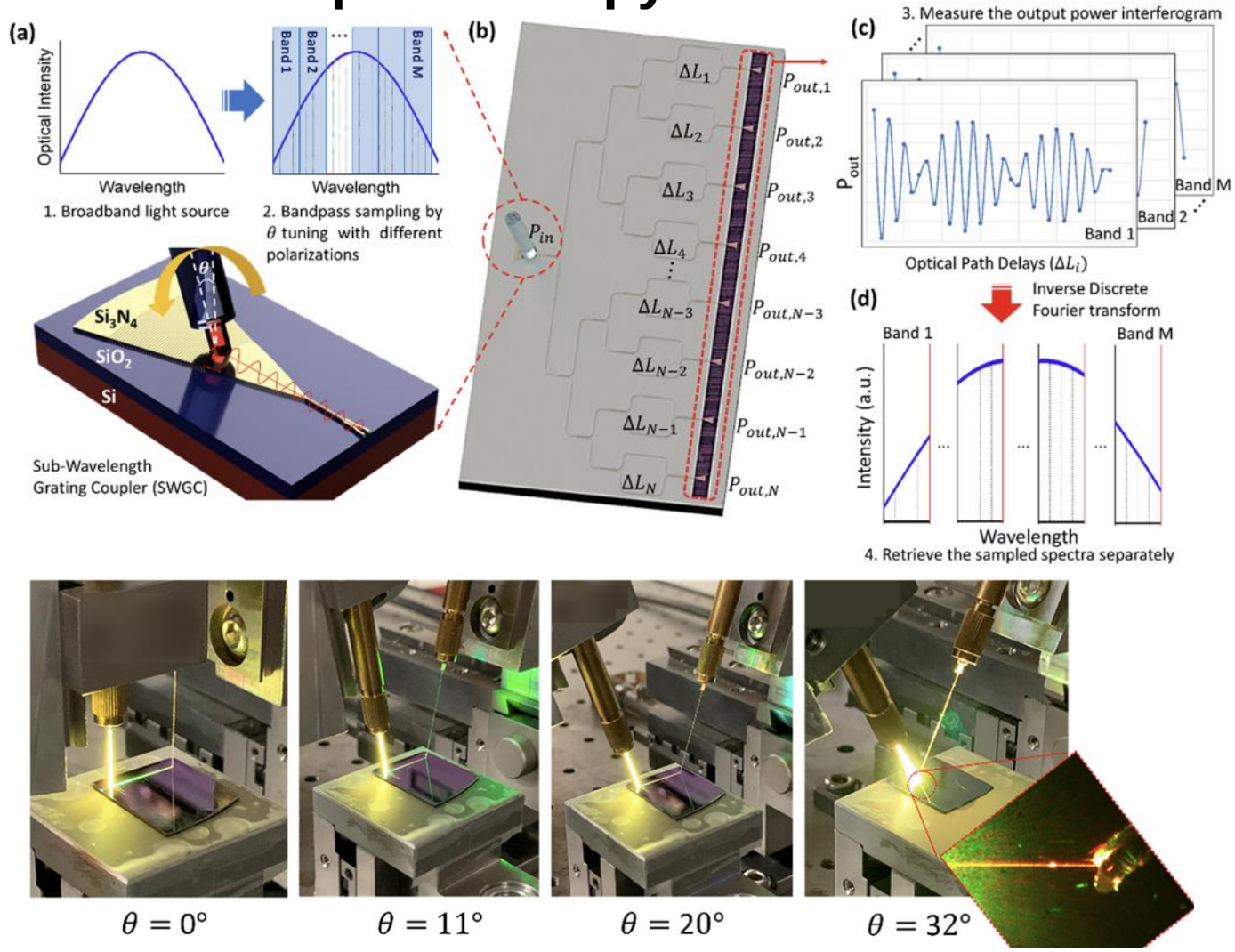

Yoo, Kyoung Min, and Ray T. Chen. ACS photonics 9.8 (2022): 2691-2701.

Device Fabrication

- **After EBL**

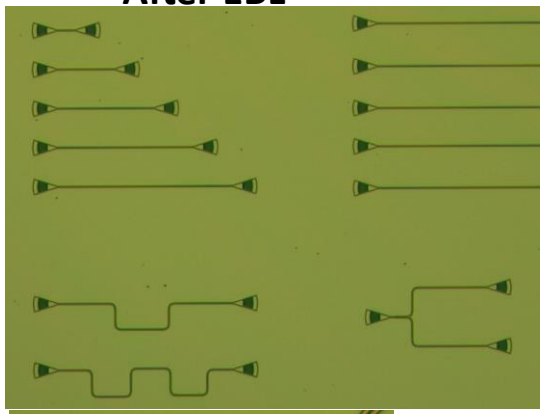

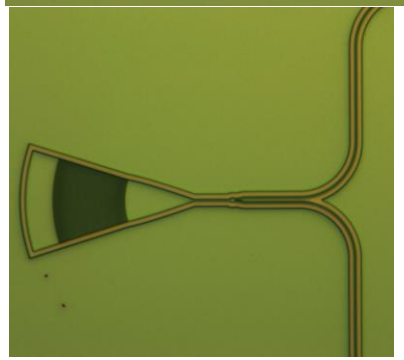

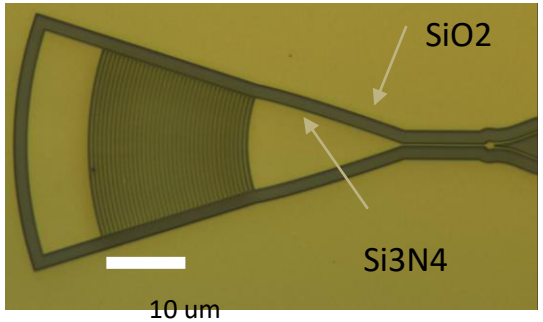

- **After Si3N4 etching**

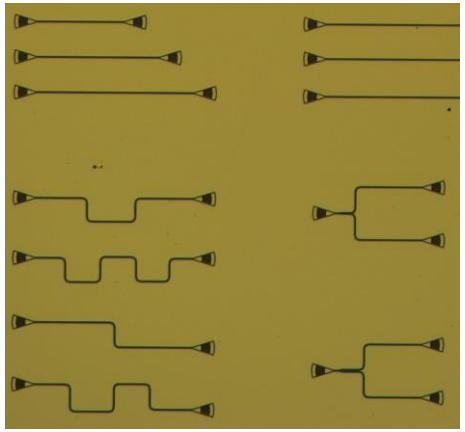

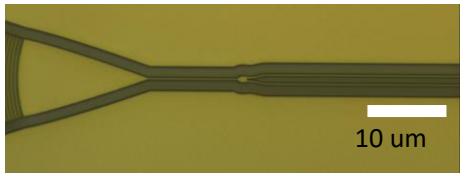

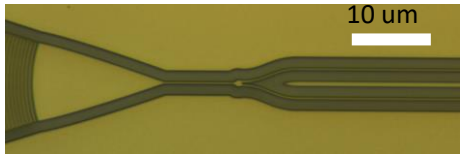

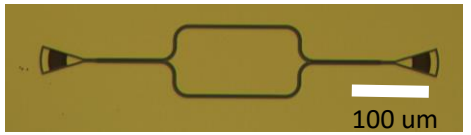

MZI Design parameters:
Waveguide width: 500 nm
Grating period: 710 nm
Grating width: 430 nm
MZI number : 24
Maximum path delay: 106 um

- FTS measurement result

Data process (MATLAB)

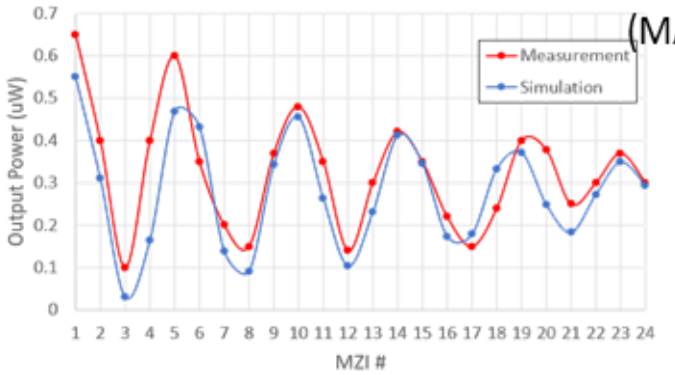

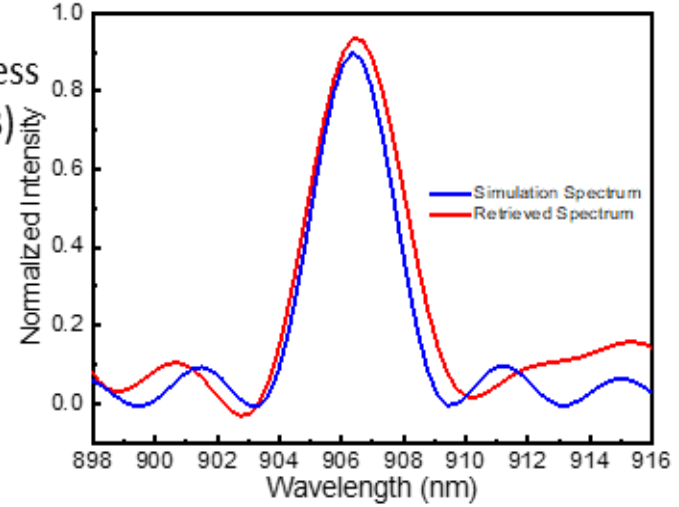

Table of Contents:

Free-space optical technologies – why mid-infrared?

Hence: Operation in adverse conditions such as fog, haze, and intense sunlight

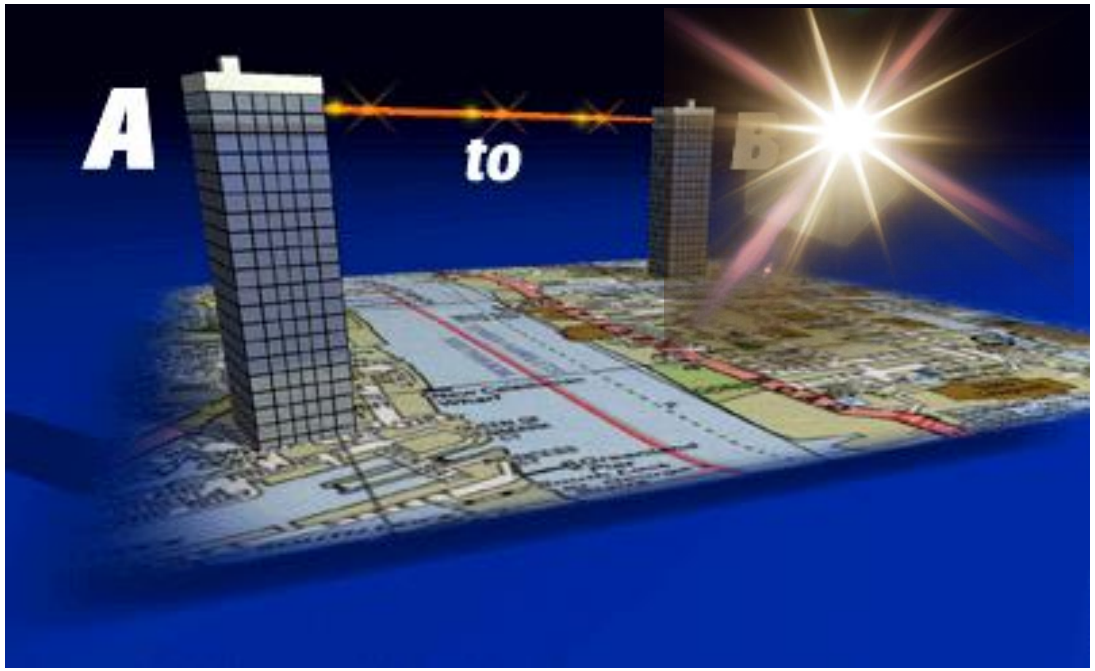

www.cablefreesolutions.com

1D Optical Phased Array – beam forming and steering

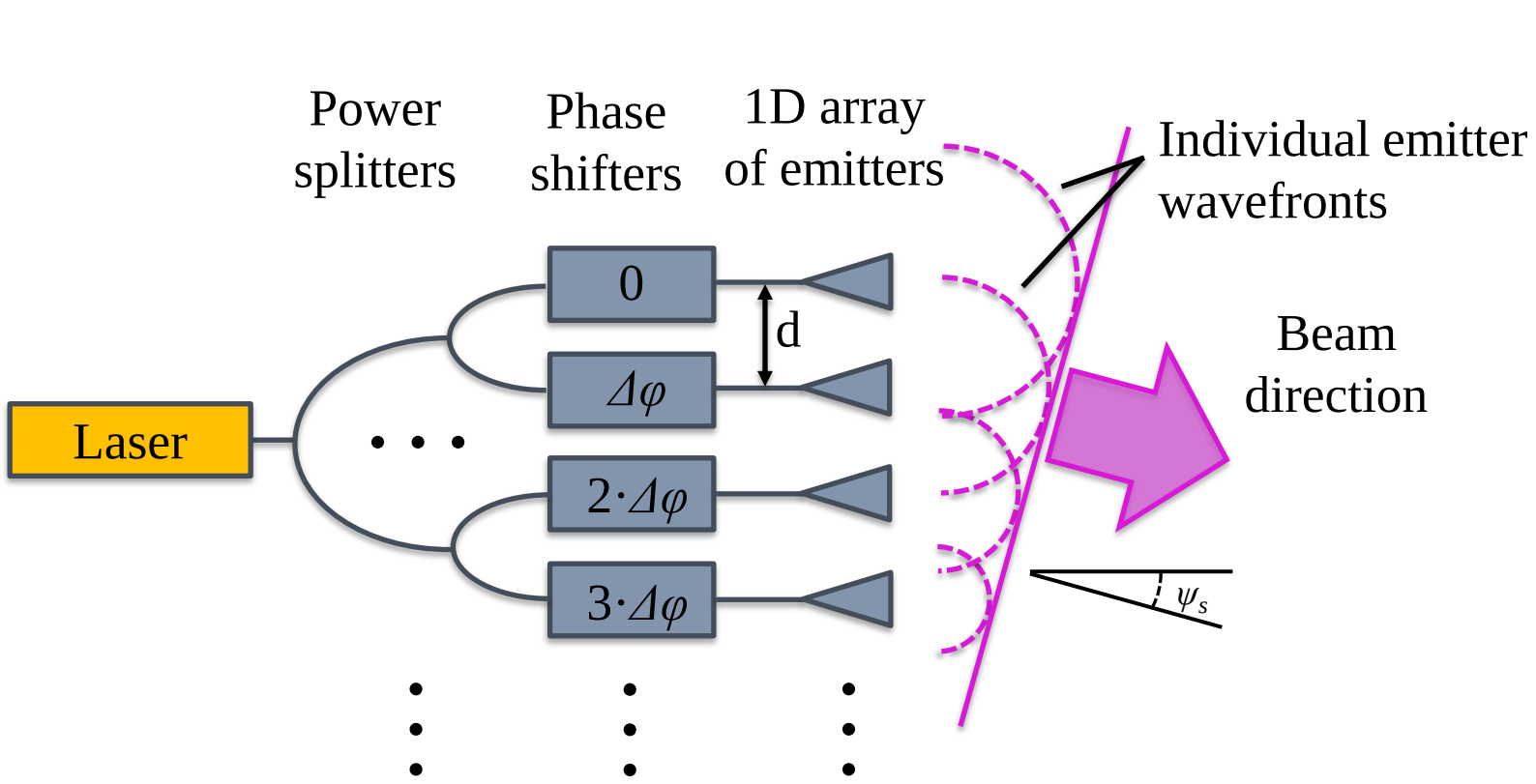

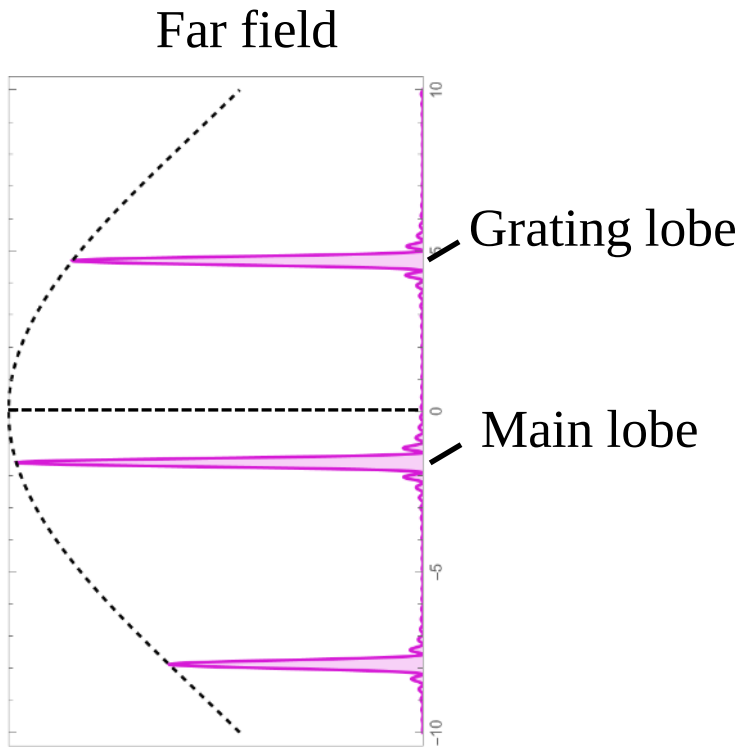

$$\sin\psi_s = \frac{\Delta\varphi}{2\pi}\frac{\lambda}{d}$$

$$\sin\psi - \sin\psi_s = \frac{m\lambda}{d}, \quad m = 0, \pm 1, \ldots$$

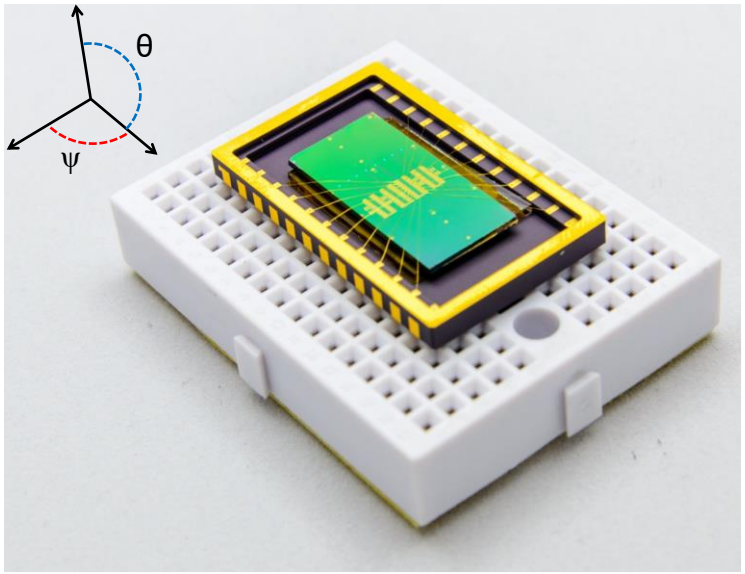
θ
ψ

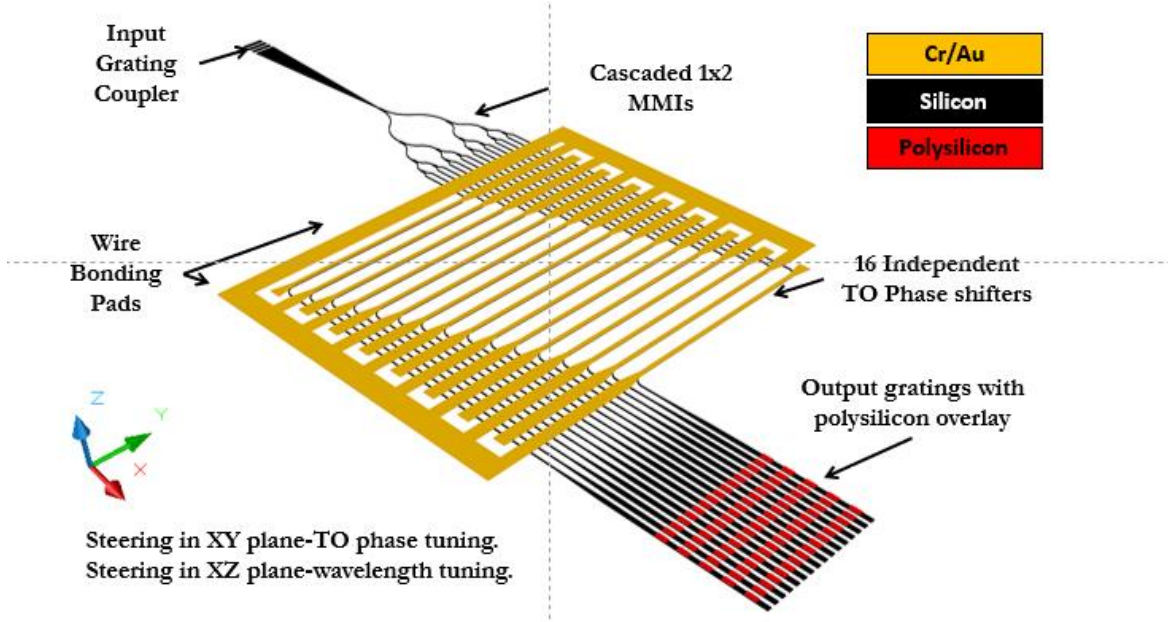
Input Grating Coupler
Cascaded 1x2 MMIs
Cr/Au
Silicon
Polysilicon
Wire Bonding Pads
16 Independent TO Phase shifters
Output gratings with polysilicon overlay
Z
Y
X
Steering in XY plane-TO phase tuning.
Steering in XZ plane-wavelength tuning.

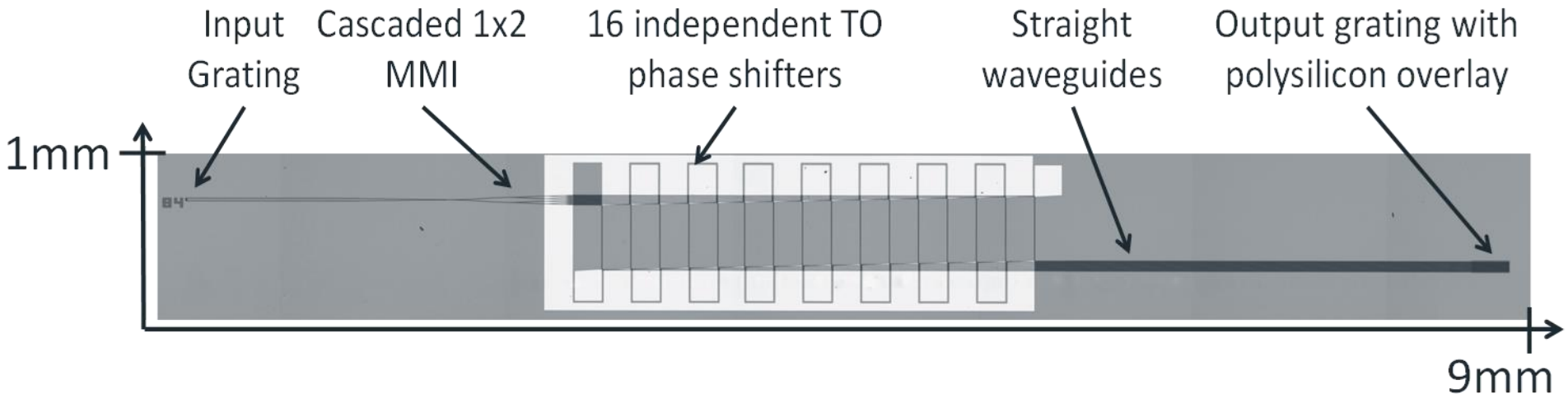
Input Grating
Cascaded 1x2 MMI
16 independent TO phase shifters
Straight waveguides
Output grating with polysilicon overlay
1mm
9mm

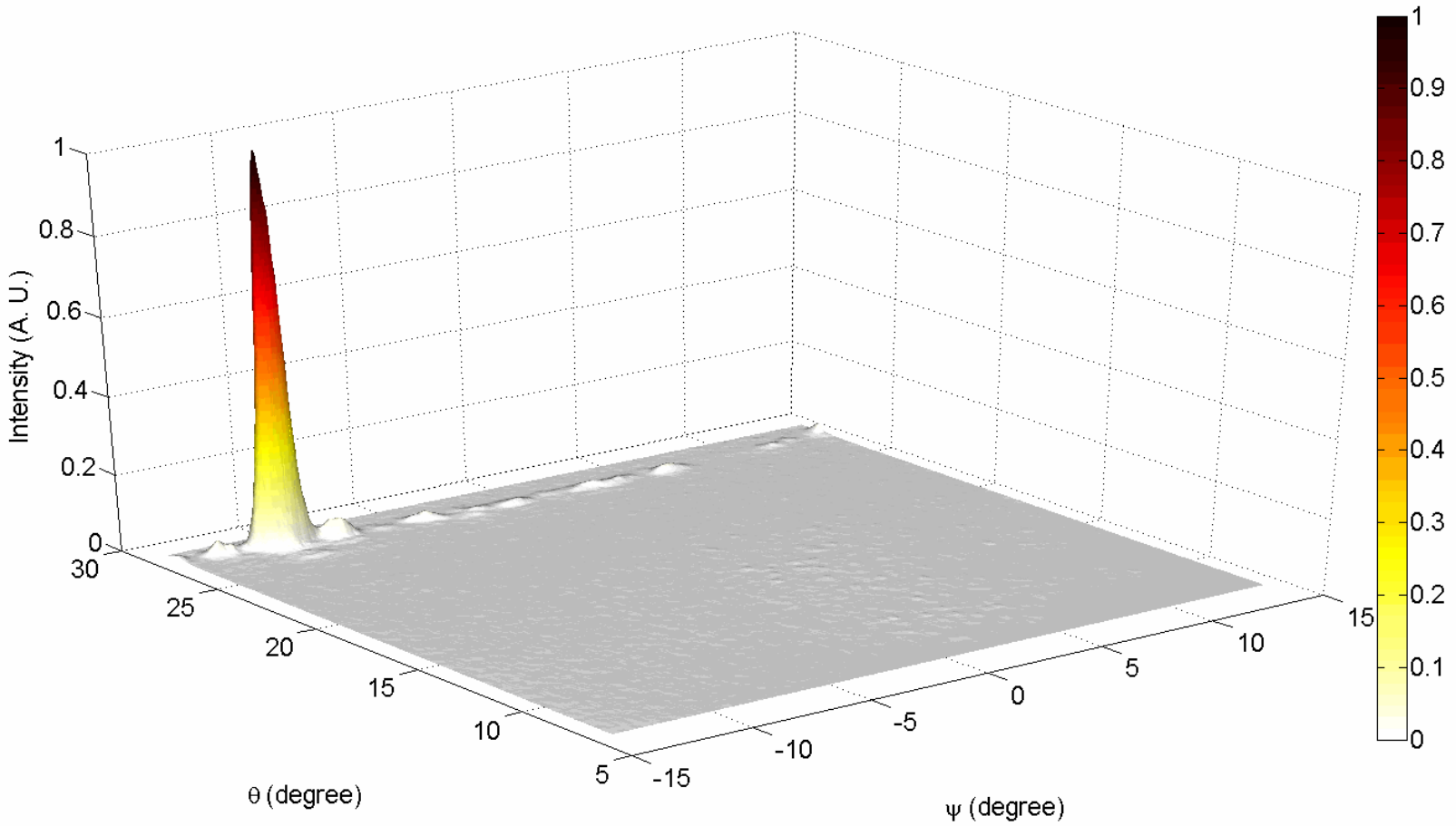
Intensity (A. U.)
1
0.8
0.6
0.4
0.2
0
30
25
20
15
10
5
θ (degree)
-15
-10
-5
0
5
10
15
ψ (degree)
1
0.9
0.8
0.7
0.6
0.5
0.4
0.3
0.2
0.1
0

1D Optical Phased Array – demonstration @ λ = 4.6 μm

Power splitters

Thermo-optic phase shifters

Emission gratings

L

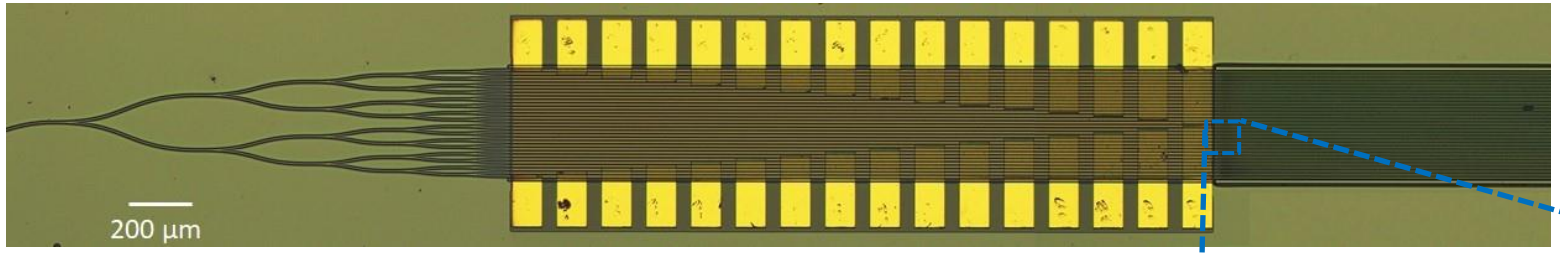

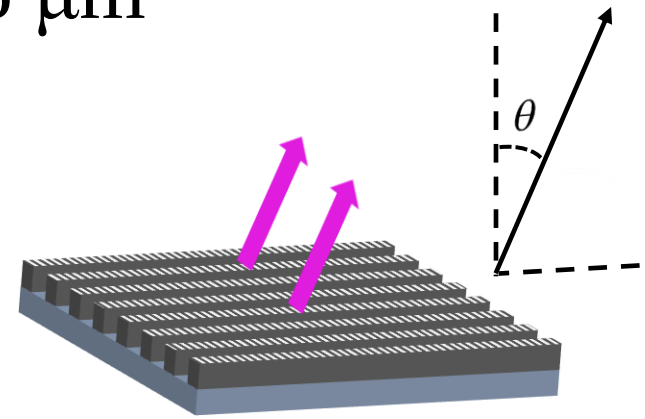

$$\sin\theta = n_{eff} - \frac{\lambda}{\Lambda}$$

$$\theta \approx 5°$$

InGaAs/InP

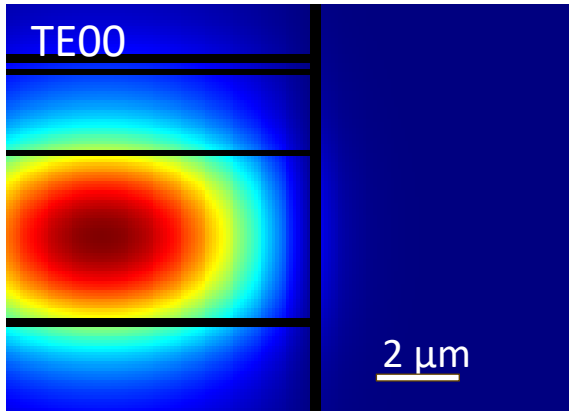

$$\Delta\varphi = \frac{2\pi}{\lambda} L \frac{dn_{eff}}{dT} \Delta T$$

$$\frac{dn_{eff}}{dT} \approx 2 \times 10^{-4} \mathrm{K}^{-1}$$

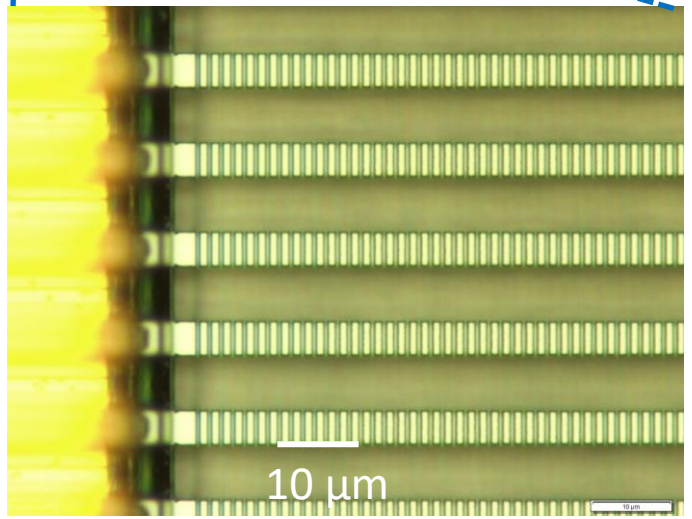

Midkiff et al., *Optica* 7, 11, 1544 (2020).

2D Optical Phased Array – beam forming and steering

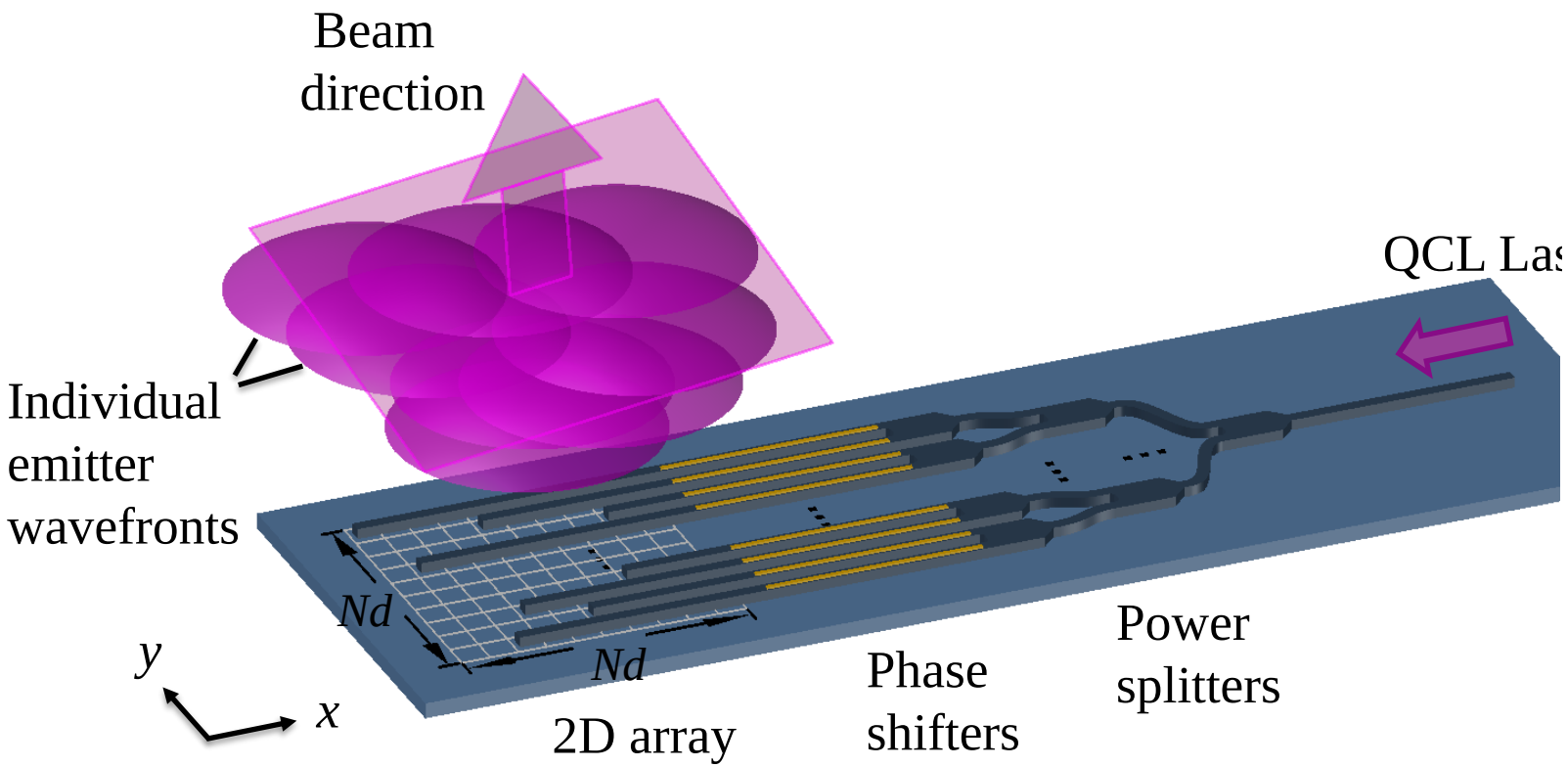

Far field
(within the unambiguous steering range)

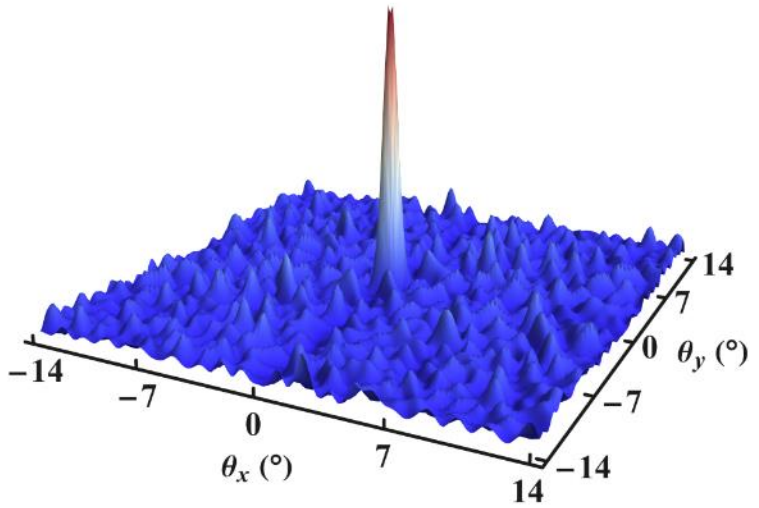

$$\sin\psi_{sx} = \frac{\Delta\varphi_x}{2\pi}\frac{\lambda}{d} \qquad \sin\psi_{sy} = \frac{\Delta\varphi_y}{2\pi}\frac{\lambda}{d}$$

$$\sin\psi_x - \sin\psi_{sx} = \frac{m_x\lambda}{d}, \quad m_x = 0, \pm 1, \ldots$$

$$\sin\psi_y - \sin\psi_{sy} = \frac{m_y\lambda}{d}, \quad m_y = 0, \pm 1, \ldots$$

2D Optical Phased Array – element distribution (2λ-spaced uniform grid)

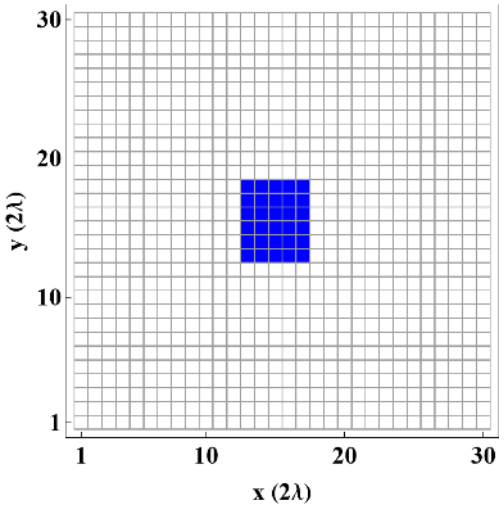

30 elements,
tightly packed

- FOV: 28° × 28°
- BW: 3.7° × 4.5°
- ➢ 47 resolvable points
- ➢ PSLL = -28 dB

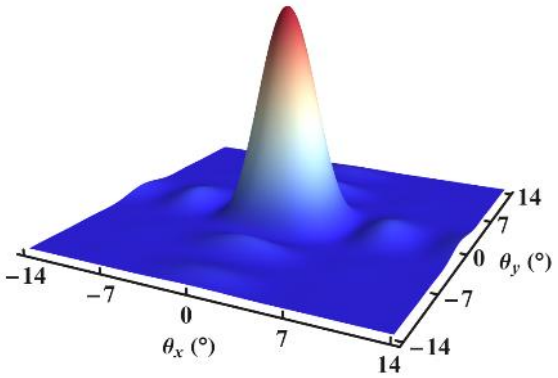

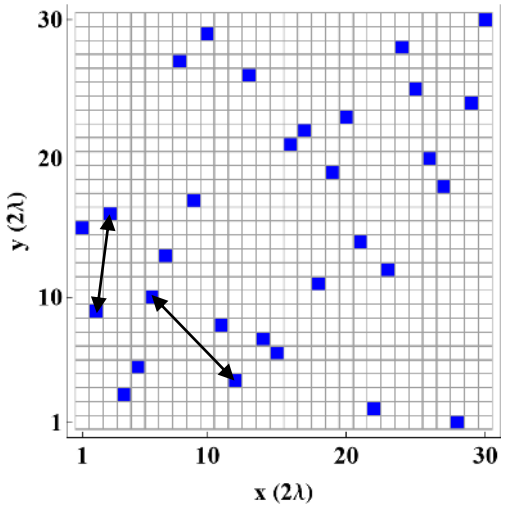

30 elements,
sparse non-redundant

- FOV: 28° × 28°
- BW: 0.6° × 0.6°
- ➢ 2177 resolvable points
- ➢ PSLL = -17 dB

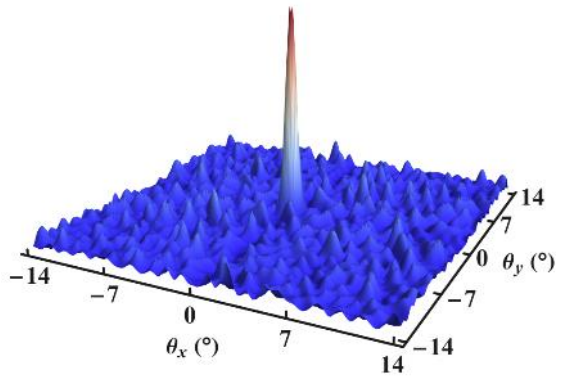

2D Optical Phased Array – demonstration @ λ = 4.6 μm

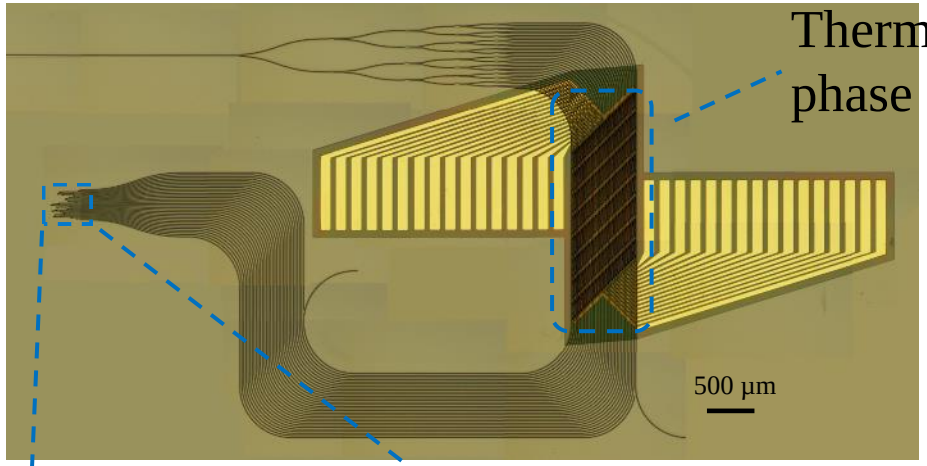

Emitter array

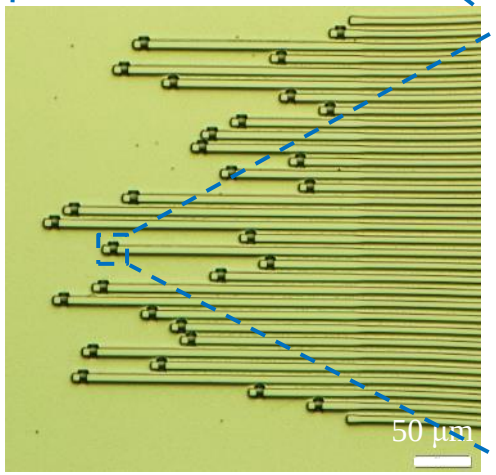

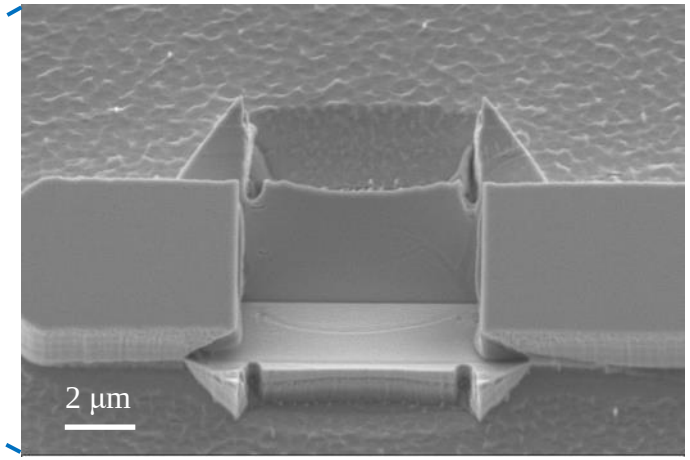

TIR Mirror Emitter

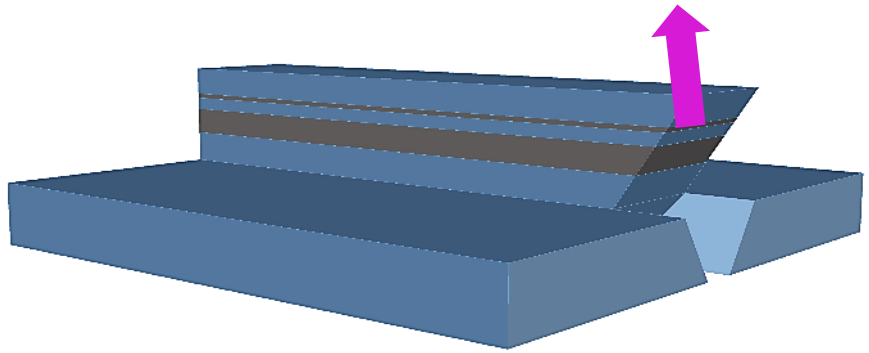

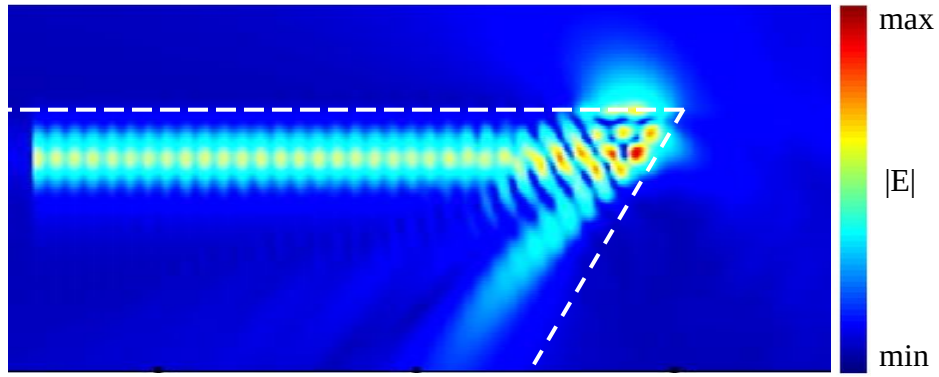

2D Optical Phased Array – demonstration @ λ = 4.6 μm

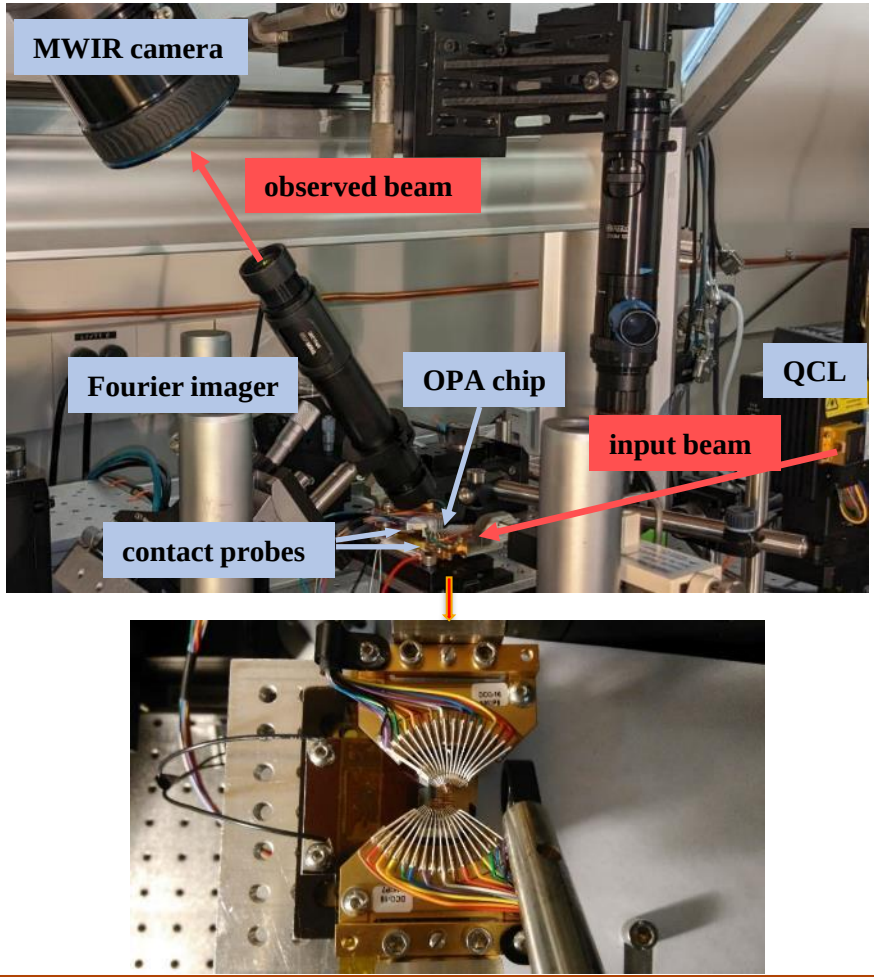

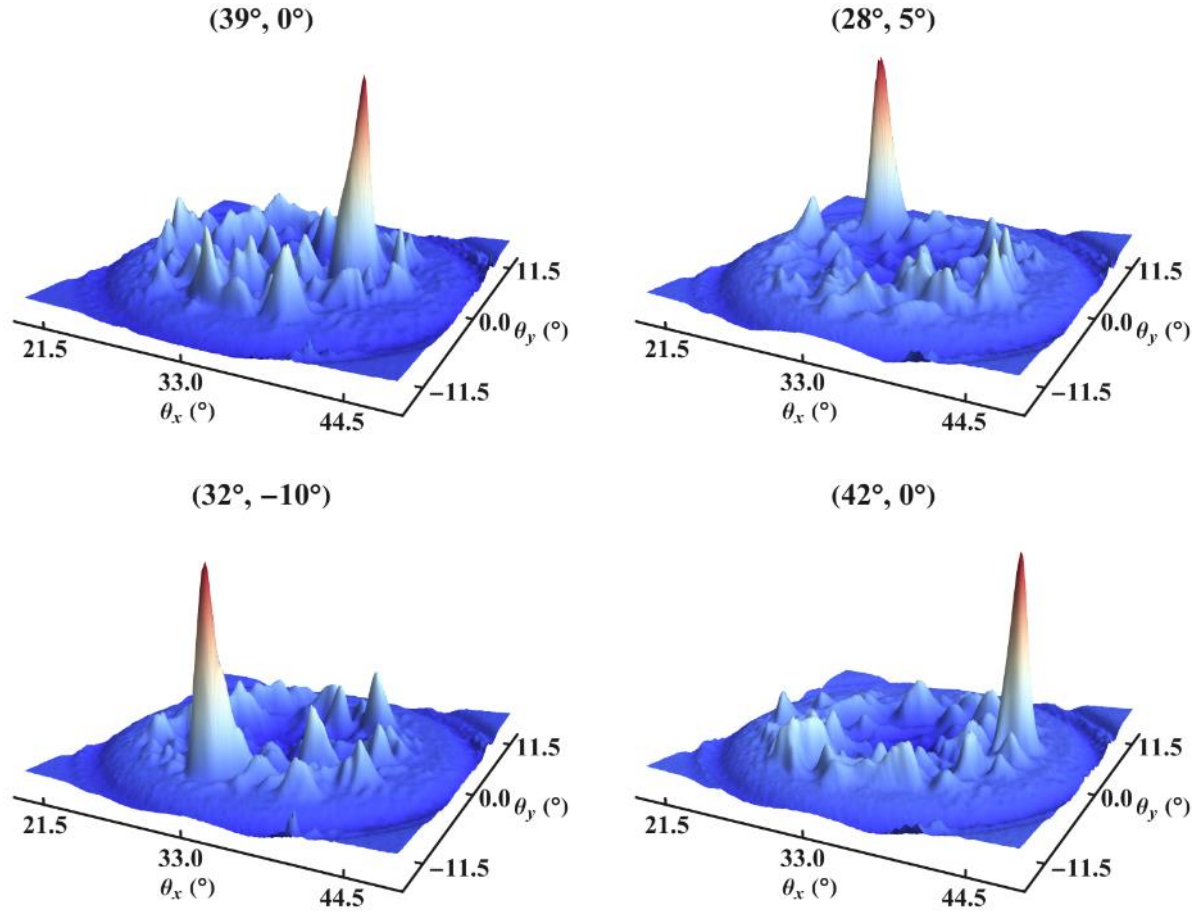

resolution: $\cong \frac{28.1° \times 28.2°}{0.86° \times 0.74°} = 1246$ resolvable points

MODTRAN Simulations of Transmittance vs Visibility for Typical and Proposed Experimental Setup of Mid-IR 2D-Scanning Lidar System

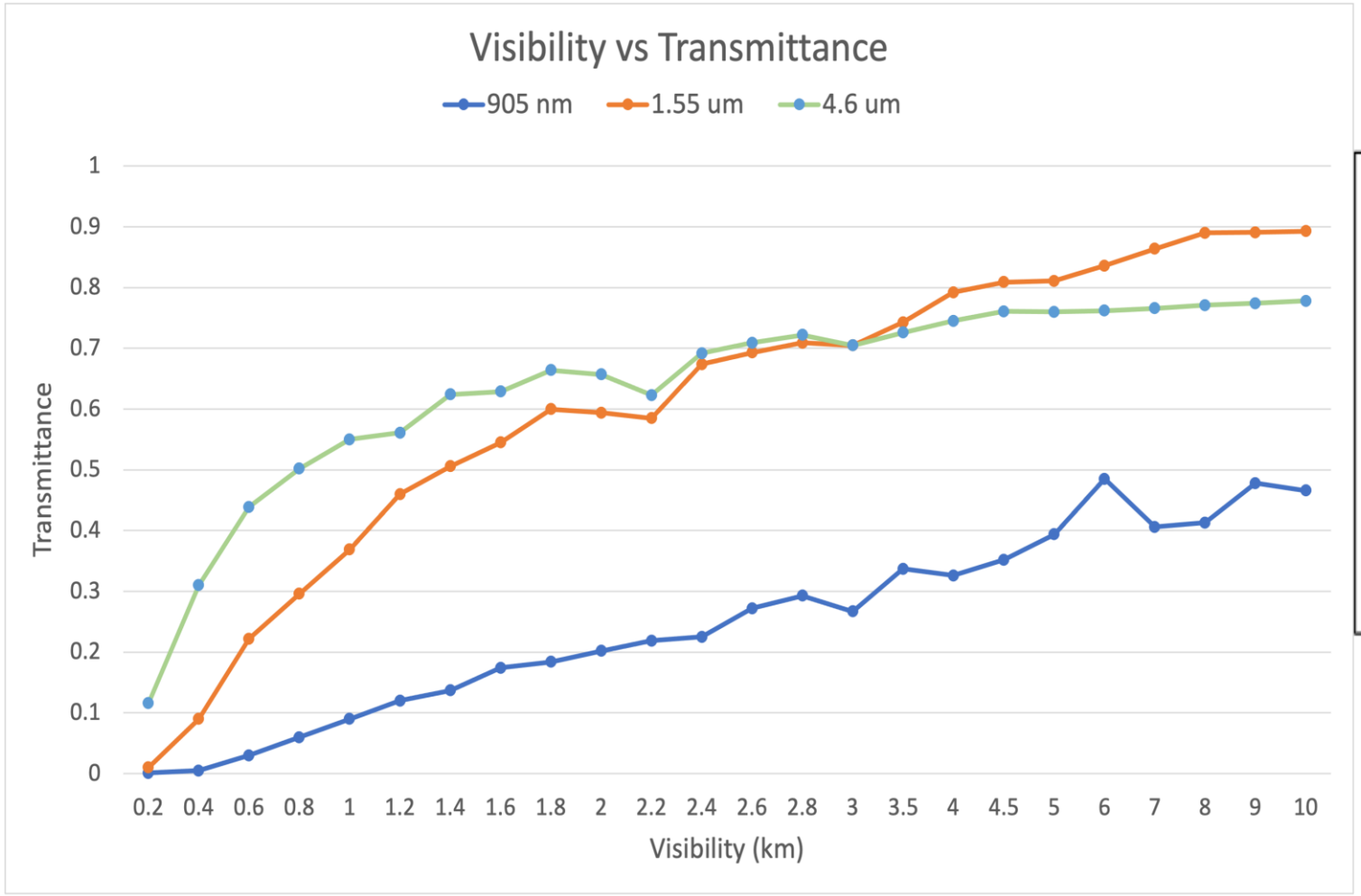

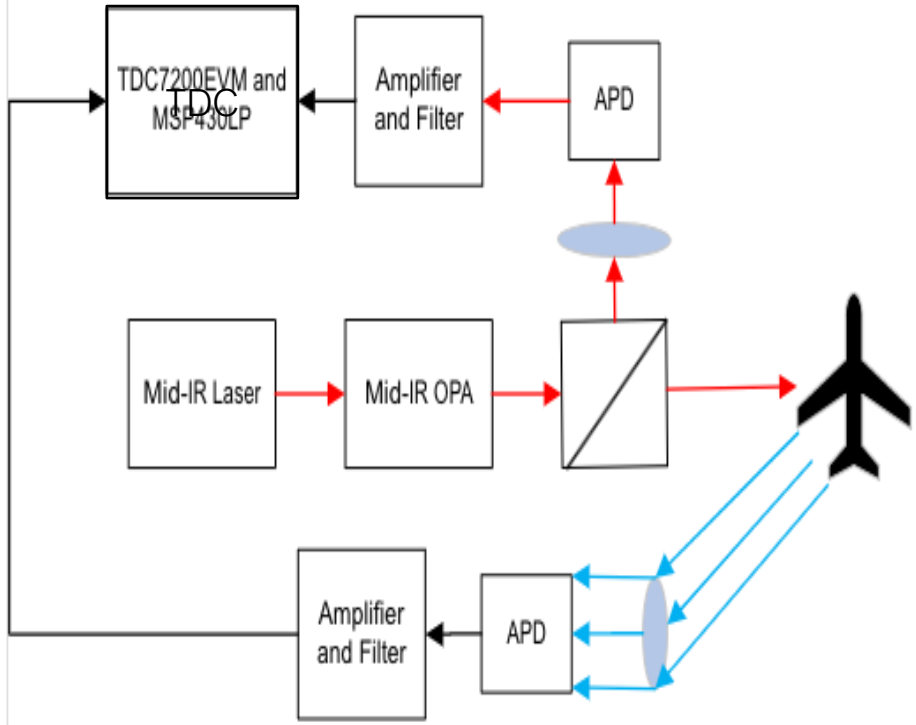

Table of Contents:

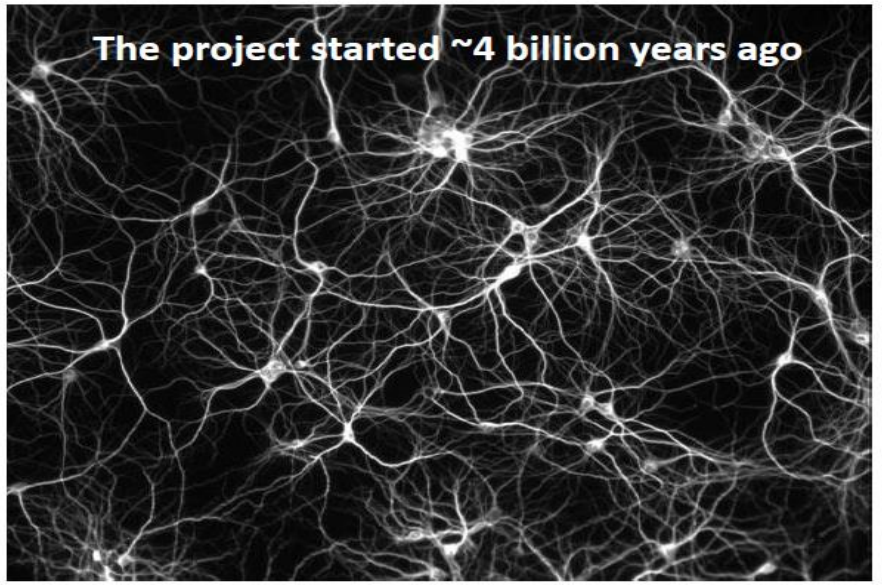

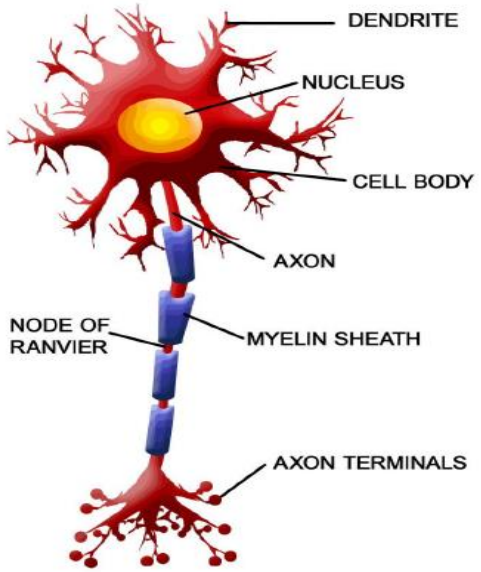

Feedforward network

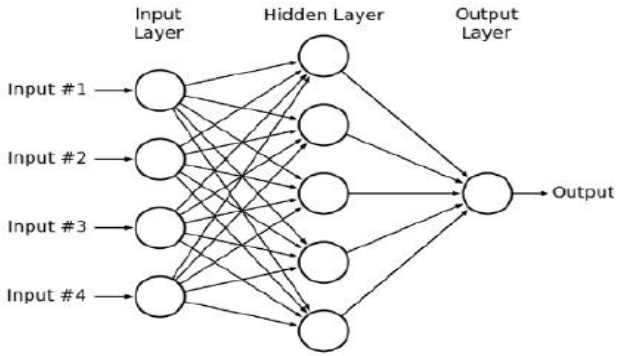

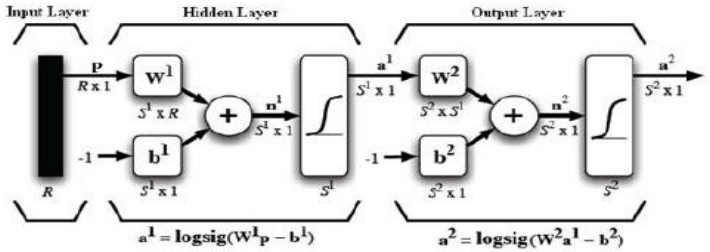

Recurrent network

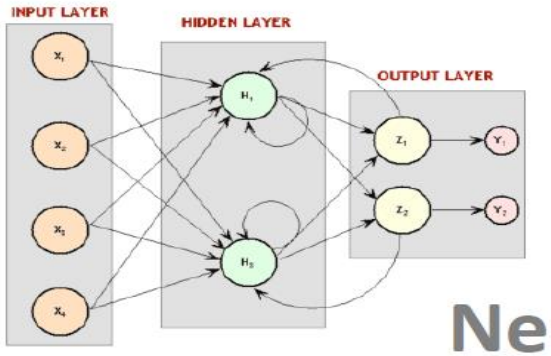

Echo state network

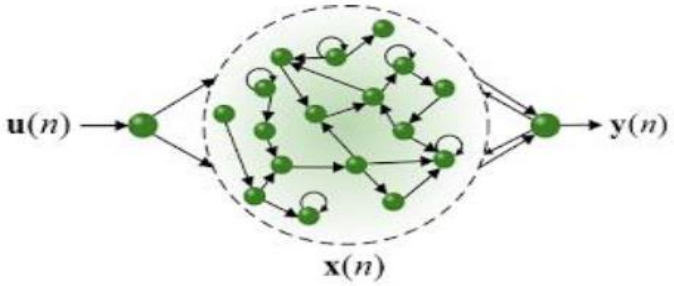

Neuromorphic Computing

Photonic AI keeps growing

Why Photonic AI ?

- Low latency and low power consumption
- High bandwidth in the **analog** domain
- Unique multiplexing techniques, *e.g.*, **WDM**
- Integrated photonics bring new opportunities…

AI influences various aspects of our lives

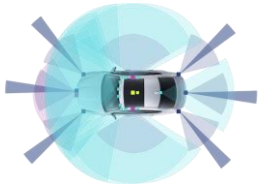

Autonomous driving

Data centers

Medical Diagnosis

ChatGPT

General Language Model

Electrical Computation

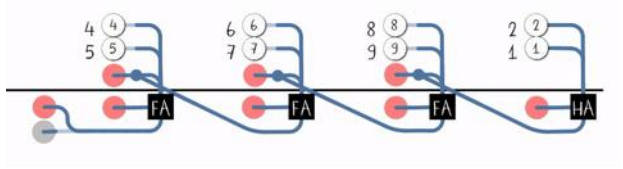

Optical Computing

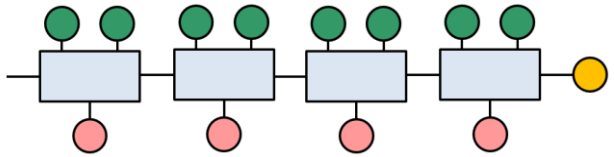

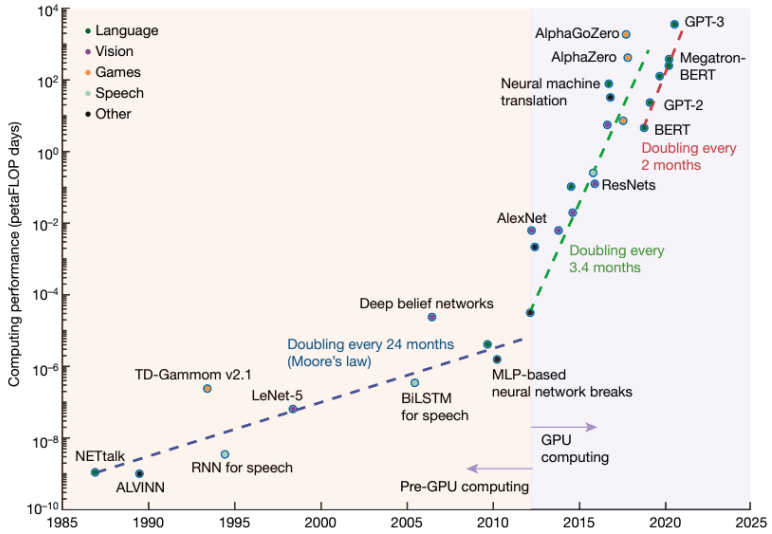

[Mehonic+, 2022]

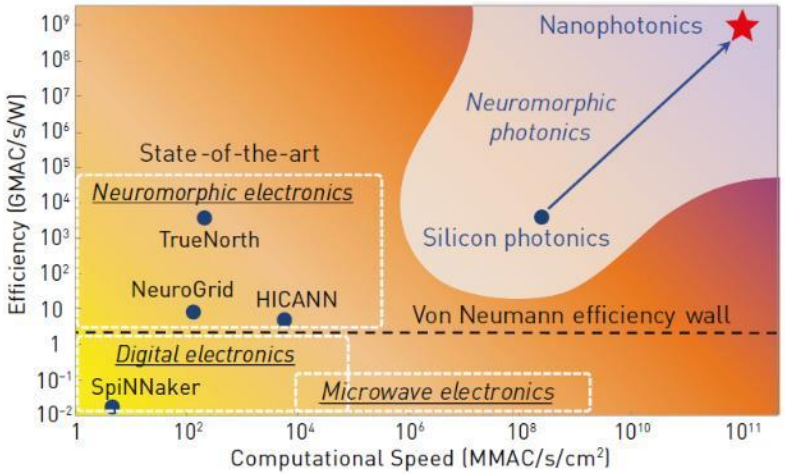

[Mitchell+, 2018]

Recent Work on Optical Neuron Networks (ONNs)

Photonic Neural Network Trends in Academia

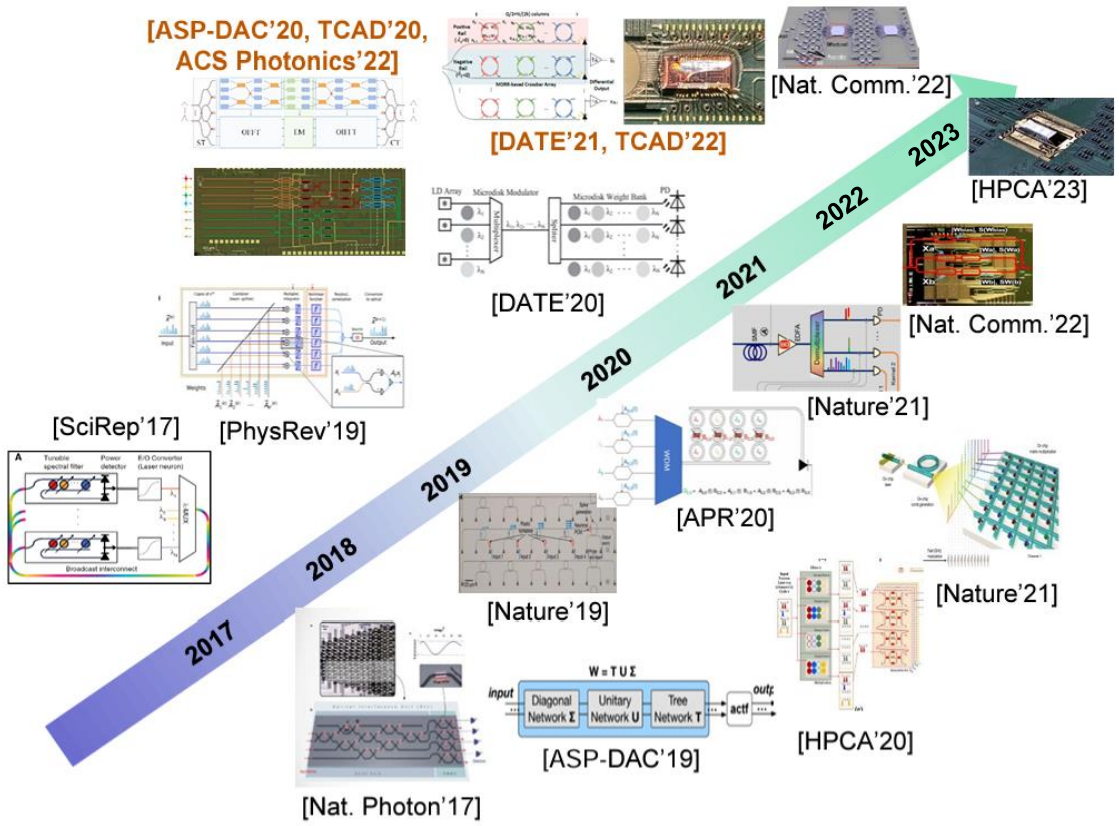

Foundry / EPDA Support in Industry

Photonic Computing Chip Designs

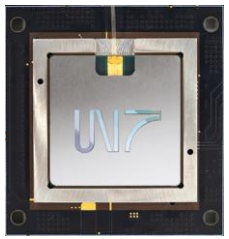

LIGHTMATTER
LIGHTELLIGENCE
SALIENCE LABS
LUMINOUS
OPTIUS light powered computing
Lighton

Design Automation / Simulation Tools

Ansys LUMERICAL
SYNOPSYS OPTICAL & PHOTONIC SOLUTIONS
cadence
COMSOL

PDKs / Foundry

amf ADVANCED MICRO FOUNDRY
AIM PHOTONICS
SiEPIC FAB OpenEBL
tsmc
GlobalFoundries

Building blocks of Analog integrated photonic AI accelerator

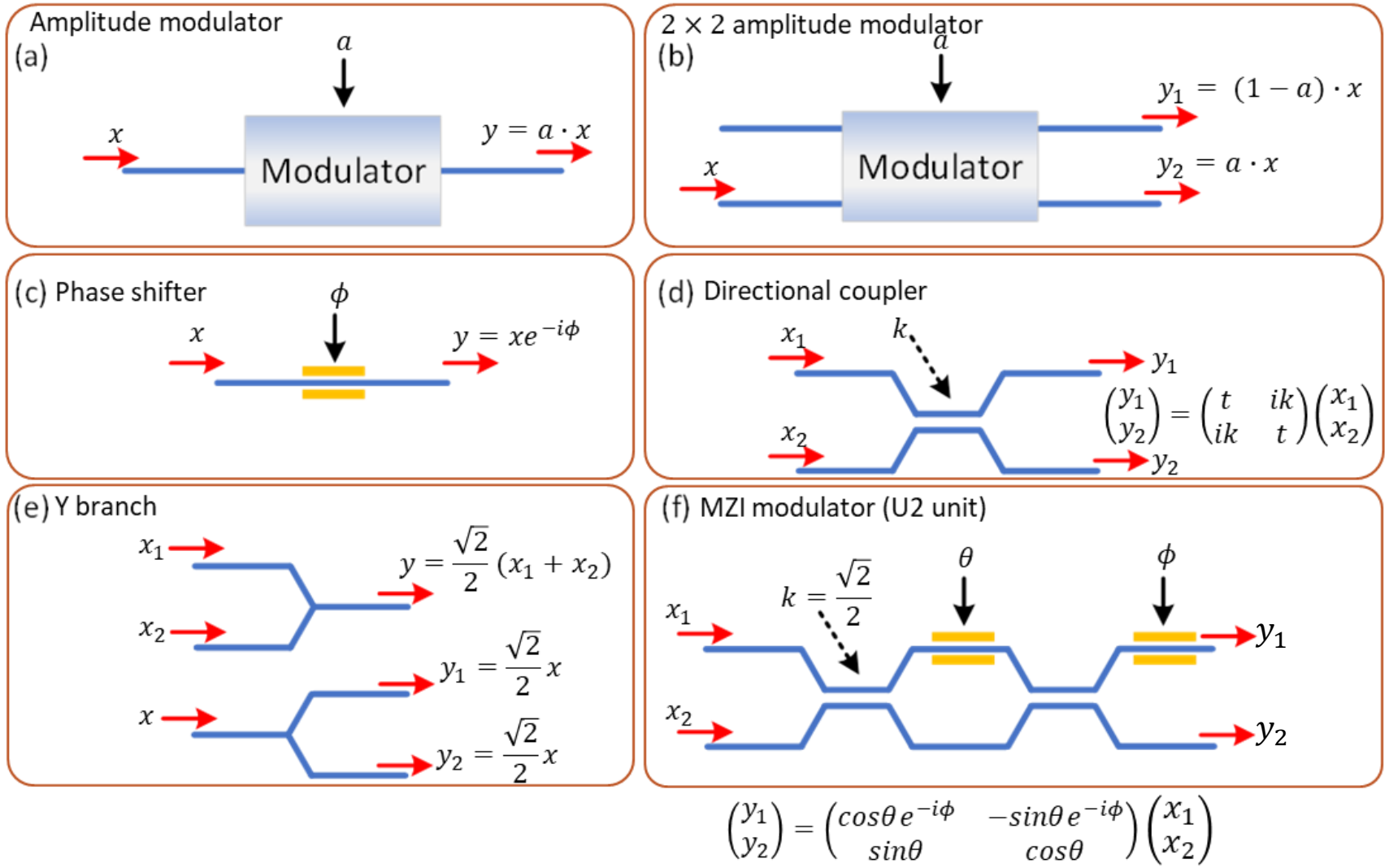

Implementation of Photonic Tensor Core (PTC)

MZI Mesh based on *Singular Value Decomposition (SVD)*
[Shen+, 2017]

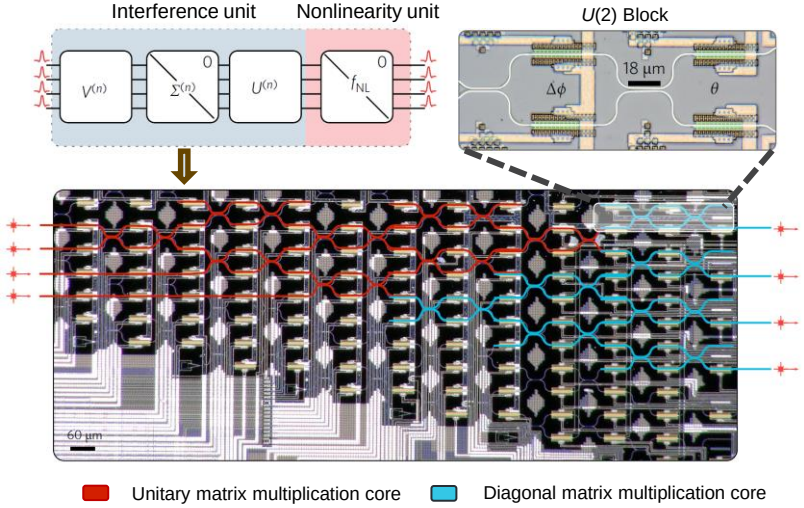

Weight Bank Architecture [Tait+, 2017]

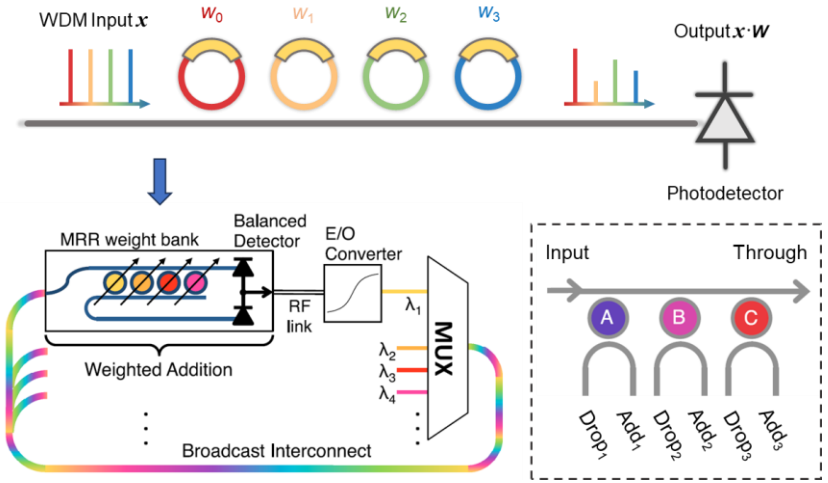

PCM-based All-optical Spiking Neuron
[Feldmann+, 2017]

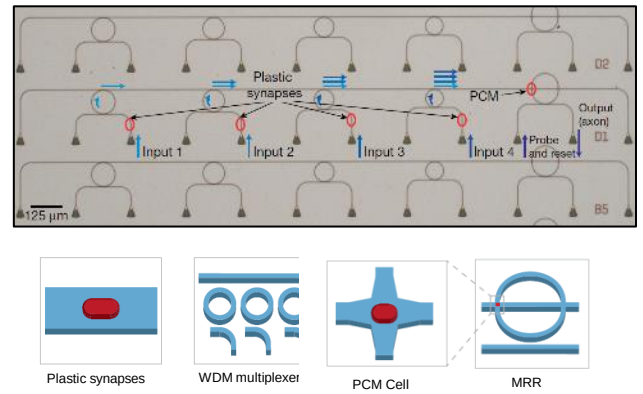

Full-range Dot-product based on Coherent Interference
[Shen+, 2017]

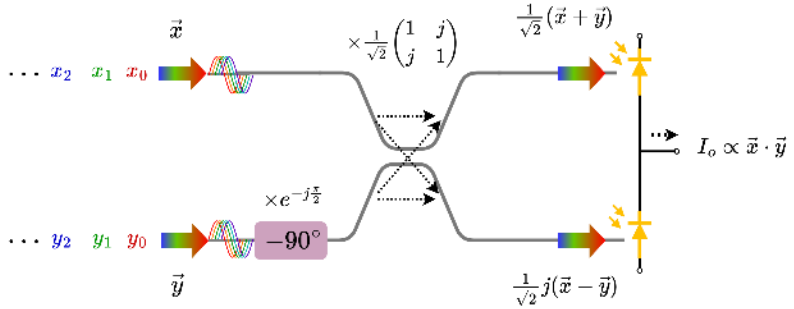

MRR-based Crossbar Array [Ohno+, 2017]

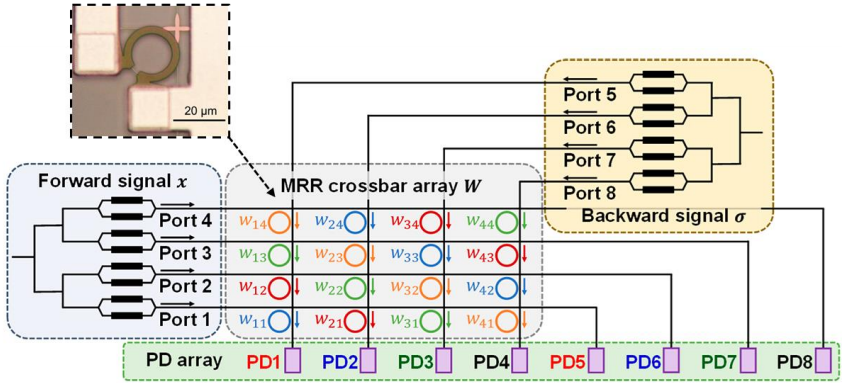

Scaling issues of ONN architectures

- Hardware complexity for modulation
  # of device $O(m^2 + n^2)$ or $O(m \cdot n)$ for GEMM
- Power assumption of active devices and ADC/DAC
- High cascaded propagation loss
- High control precision requirement
- Robustness concern: Process variations, limited resolution of tunable devices, dynamic noises…

Scaling approaches of photonic-electronic AI accelerators

Device level: *Explore customized device*

Passive Device/Structure

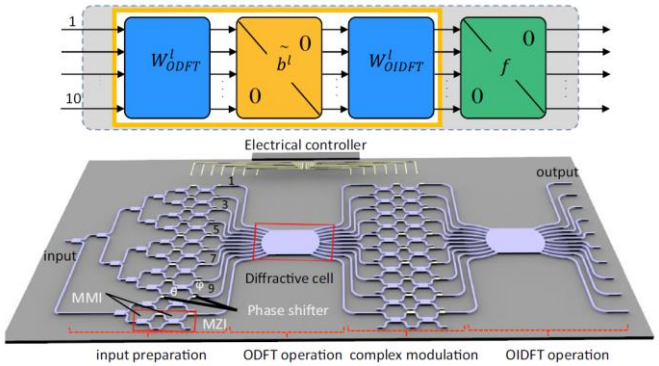

[Zhu+, 2022]

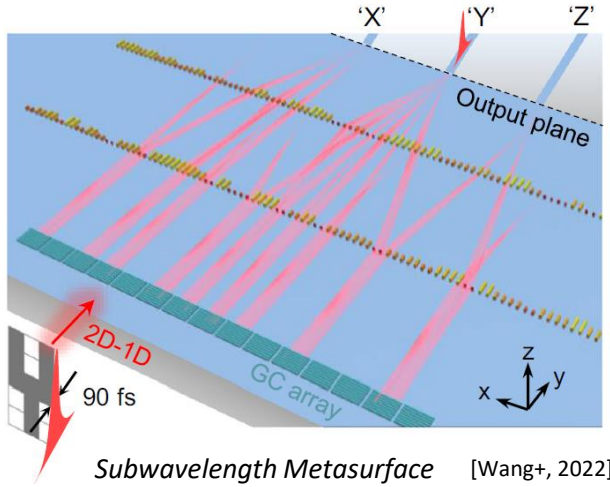

Subwavelength Metasurface [Wang+, 2022]

Multi-Operand Optical Neuron (MOON)

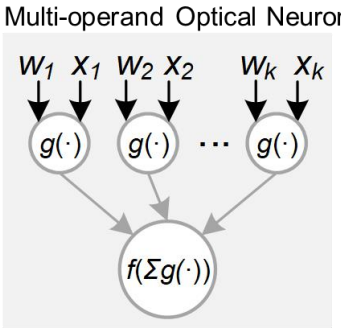

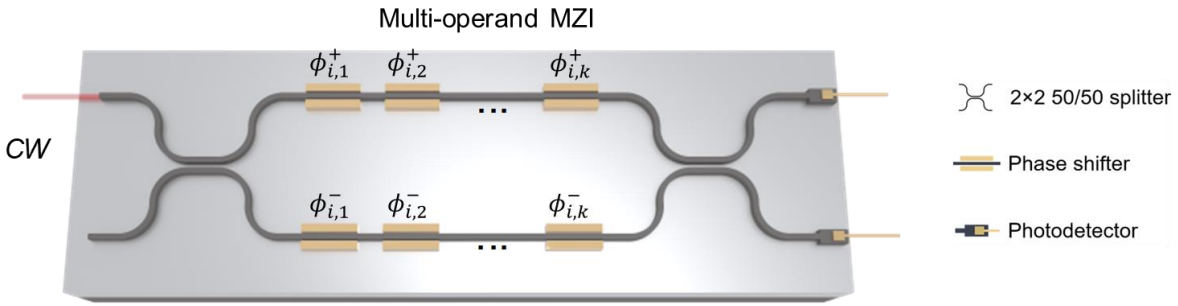

[*Feng, et al. Nanophotonics 0 (2024)*]

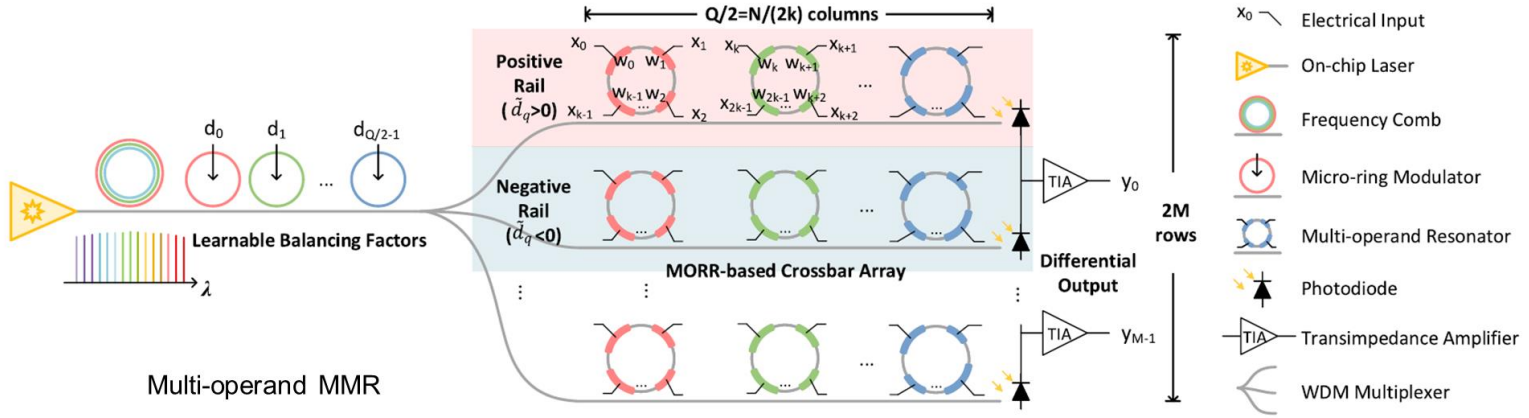

[*Gu, et al. 2021 Design, Automation & Test in Europe Conference & Exhibition (DATE). IEEE, 2021.*]

Our efforts: Four rounds of optical neural chips

2020

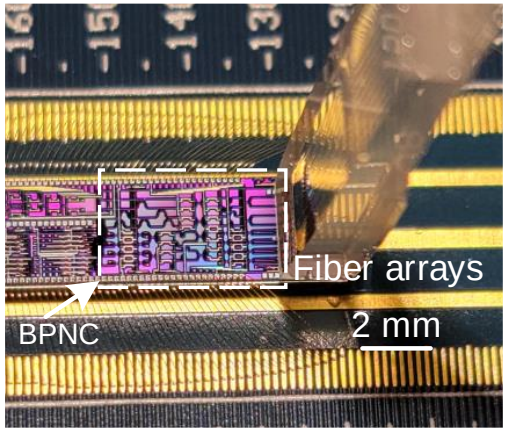

- Butterfly-style photonic circuit mesh
  [*Feng, et al. Acs Photonics 9.12 (2022)*]
- ➢ Co-packaged chips
- ➢ Electrical control systems for analog computing

2022

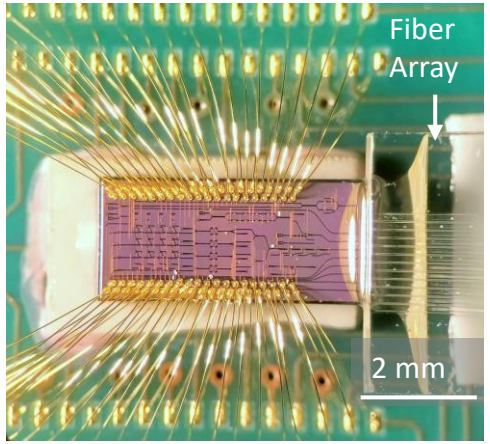

- Multi-operand optical neurons
  [*Feng, et al. Nanophotonics 0 (2024)*]
- Block-circulant subspace ONN
  [*Ning, et al. SPIE, 2024*]
- ➢ On-chip photodetection
- ➢ Customized photonic devices

2023

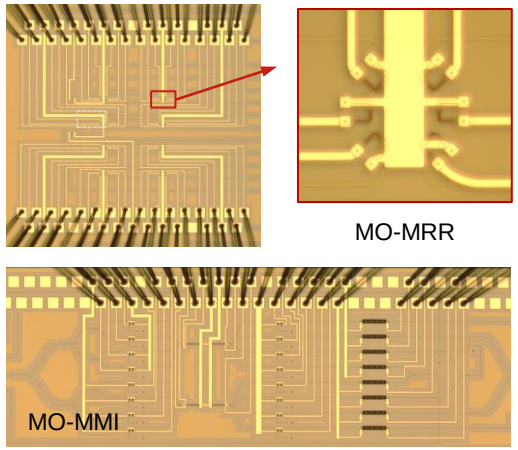

- Multi-operand-based ONNs
  [*Under Testing*]
- ➢ AI-Assisted design
- ➢ More customized devices

2024

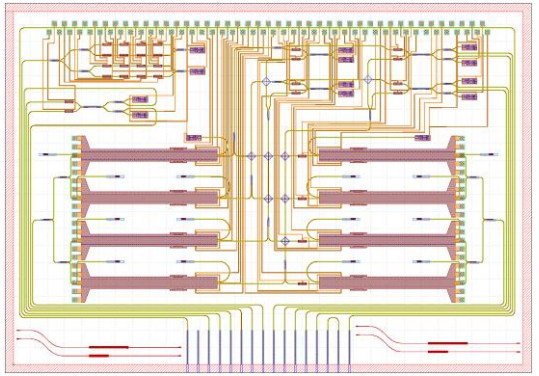

- Dynamically-operated PTC
  [*Coming this Summer*]
- ➢ Full-range MVM
- ➢ High-speed dynamically modulation

More Datasets

MNIST(handwritten digits)
>94% accuracy
DNN Model: 2-layer CNN (1.6k #params)
3-bit weight resolution

[Feng et al., ACSph, 2022]

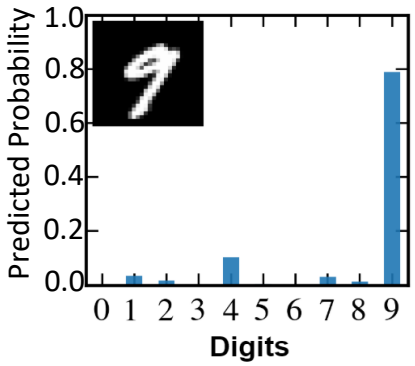

COVID Chest X-ray
96.5% accuracy
VGG8 (4M #params)
3-bit weight resolution

(For proposal use)

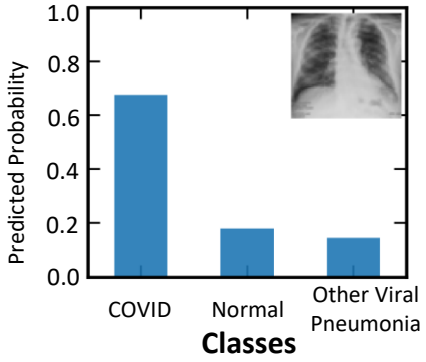

Fashion MNIST dataset
>88% accuracy
3-layer CNN
4-bit weight resolution

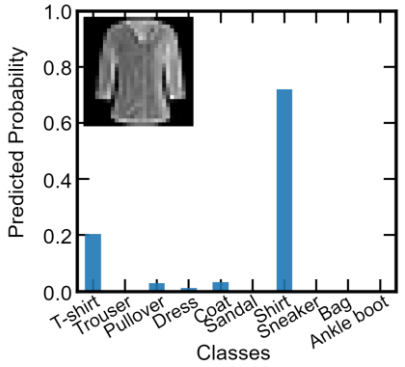

Street-view-house-number (SVHN) dataset
>85% accuracy
3-layer CNN
4-bit weight resolution
[Feng et al., Nanophotonics, 2024]

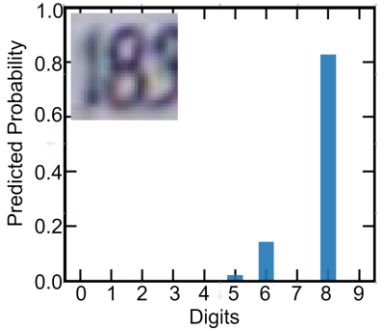

CIFAR-10 dataset
>85% accuracy on Butterfly-style PTC
3-bit weight resolution [1]

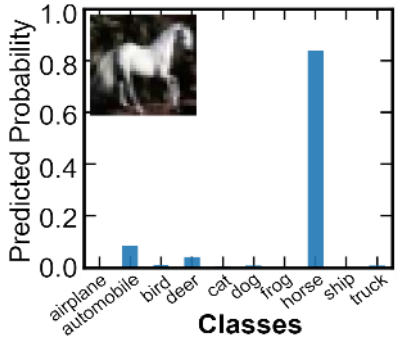

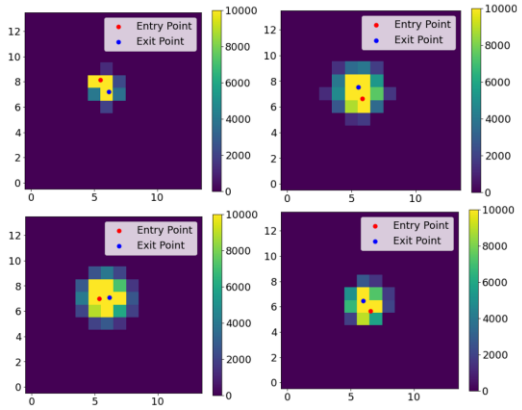

Ultracold Neutron (UCN) Dataset
<96.8% MAPE accuracy in Entry and Exit Point Prediction using OSNN

[Lin et al., ULITIMA, 2023]
[Lin et al., CLEO, 2024]

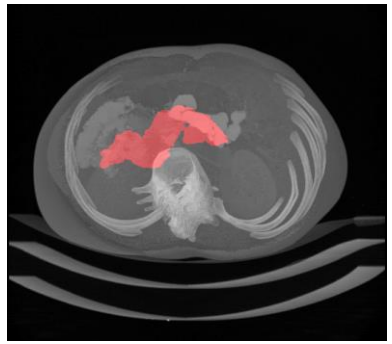

NIH Pancreas Dataset for Cancer Diagnose

3D Fully-Convolutional Network

[Yang al., CLEO, 2024]

Thank you !